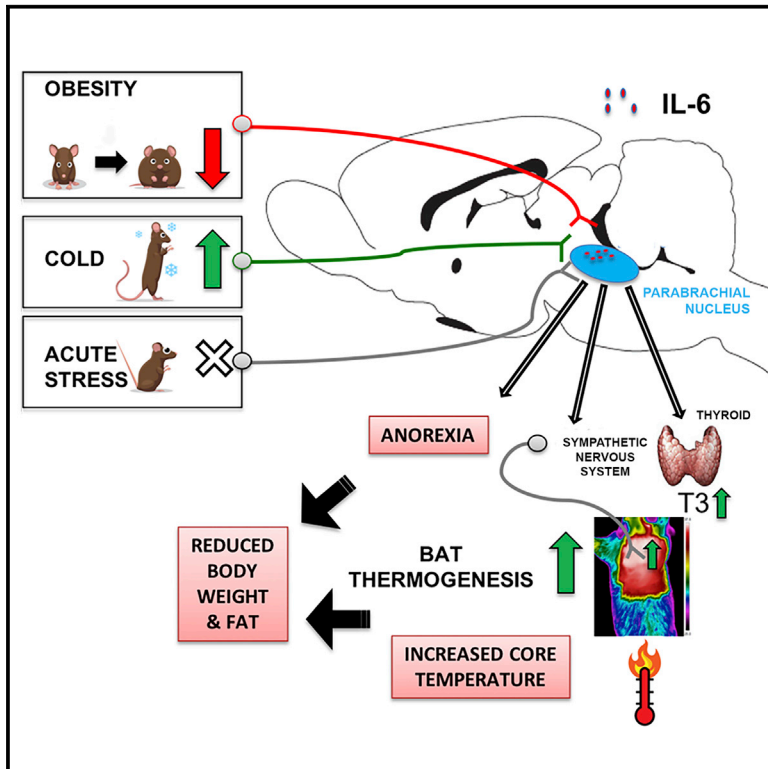# Parabrachial Interleukin-6 Reduces Body Weight and Food Intake and Increases Thermogenesis to Regulate Energy Metabolism

Graphical Abstract

Authors

Devesh Mishra, Jennifer E. Richard, Ivana Maric, ..., Harvey J. Grill, Ruben Nogueiras, Karolina P. Skibicka

Correspondence

karolina.skibicka@neuro.gu.se

In Brief

Mishra et al. demonstrate that IL-6 is produced by lPBN neurons, astrocytes, and microglia. They show that IL-6 acts in the lPBN to reduce body weight by increasing thermogenesis and reducing food intake. They also identify two pathophysiological/physiological contexts, obesity and cold exposure, that divergently affect lPBN IL-6 production.

Highlights

- Obesogenic diet robustly reduces, and 4°C cold exposure increases, rodent lPBN IL-6

- IL-6 interacts with leptin at the level of the lPBN to reduce food intake

- LPBN IL-6 leads to increased BAT thermogenesis by thyroid and sympathetic mechanisms

- Reduction in lPBN IL-6 increases weight gain and adiposity

CellPress

Cell Reports
Article

Parabrachial Interleukin-6 Reduces Body Weight and Food Intake and Increases Thermogenesis to Regulate Energy Metabolism

Devesh Mishra,[1] Jennifer E. Richard,[1] Ivana Maric,[1] Begona Porteiro,[3,4] Martin Häring,[5] Sander Kooijman,[6,7] Saliha Musovic,[1] Kim Eerola,[1] Lorena López-Ferreras,[1] Eduard Peris,[1] Katarzyna Grycel,[1] Olesya T. Shevchouk,[1] Peter Micallef,[1] Charlotta S. Olofsson,[1] Ingrid Wernstedt Asterholm,[1] Harvey J. Grill,[8] Ruben Nogueiras,[3,4] and Karolina P. Skibicka[1,2,9,*]

[1]Department of Physiology and Metabolic Physiology, Institute of Neuroscience and Physiology, The Sahlgrenska Academy at the University of Gothenburg, Gothenburg, Sweden
[2]Wallenberg Centre for Molecular and Translational Medicine, University of Gothenburg, Gothenburg, Sweden
[3]Department of Physiology, CIMUS, University of Santiago de Compostela-Instituto de Investigación Sanitaria, Santiago de Compostela, 15782, Spain
[4]CIBER Fisiopatología de la Obesidad y Nutrición (CIBERobn), 15706, Spain
[5]Division of Molecular Neurobiology, Department of Medical Biochemistry and Biophysics, Karolinska Institute, Stockholm, Sweden
[6]Department of Medicine, Division of Endocrinology, Leiden University Medical Center, 2333 ZA Leiden, the Netherlands
[7]Einthoven Laboratory for Experimental Vascular Medicine, Leiden University Medical Center, 2333 ZA Leiden, the Netherlands
[8]Lynch Laboratory, Department of Psychology, University of Pennsylvania, Philadelphia, PA 19104, USA
[9]Lead Contact
*Correspondence: karolina.skibicka@neuro.gu.se
https://doi.org/10.1016/j.celrep.2019.02.044

SUMMARY

Chronic low-grade inflammation and increased serum levels of the cytokine IL-6 accompany obesity. For brain-produced IL-6, the mechanisms by which it controls energy balance and its role in obesity remain unclear. Here, we show that brain-produced IL-6 is decreased in obese mice and rats in a neuro-anatomically and sex-specific manner. Reduced IL-6 mRNA localized to lateral parabrachial nucleus (lPBN) astrocytes, microglia, and neurons, including paraventricular hypothalamus-innervating lPBN neurons. IL-6 microinjection into lPBN reduced food intake and increased brown adipose tissue (BAT) thermogenesis in male lean and obese rats by increasing thyroid and sympathetic outflow to BAT. Parabrachial IL-6 interacted with leptin to reduce feeding. siRNA-mediated reduction of lPBN IL-6 leads to increased weight gain and adiposity, reduced BAT thermogenesis, and increased food intake. Ambient cold exposure partly normalizes the obesity-induced suppression of lPBN IL-6. These results indicate that lPBN-produced IL-6 regulates feeding and metabolism and pinpoints (patho)physiological contexts interacting with lPBN IL-6.

INTRODUCTION

Obesity is frequently accompanied by chronic low-grade inflammation and increased serum levels of interleukin-6 (IL-6), an essential component of the immune response. Elevated IL-6 levels result from increased IL-6 production in adipocytes (Roytblat et al., 2000; Stenlöf et al., 2003) and can be normalized by low-calorie diets (Bastard et al., 2000; Gallistl et al., 2001). This cytokine clearly has detrimental effects during obesity and inflammatory disorders. Reducing circulating IL-6 action, by blocking IL-6 receptors, is approved for the treatment of patients with rheumatoid arthritis and other inflammatory disorders. Yet IL-6 function may not be restricted to the immune response during disease (Benrick et al., 2009; Chida et al., 2006; Erta et al., 2012; Schéle et al., 2012); IL-6 also may be essential for the control of metabolism during health. In fact, patients receiving tocilizumab, IL-6 receptor-inhibiting monoclonal antibodies approved for clinical use, often suffer from increased weight gain and dyslipidemia (Febbraio et al., 2010). Likewise, whole-body IL-6 knockout in mice leads to increased body weight, subcutaneous fat, and dysregulation of glucose metabolism (Wallenius et al., 2002b), indicating pleiotropic role of this cytokine.

The CNS is suggested as the main site for the metabolic and anorexic effects of IL-6 (Timper et al., 2017; Wallenius et al., 2002a). Key energy balance signals, like leptin, glucagon-like peptide-1 (GLP-1), and amylin, require intact CNS IL-6 to reduce food intake and body weight (Le Foll et al., 2015; Shirazi et al., 2013; Timper et al., 2017). Peripheral and CNS IL-6 systems are possibly distinct, because elevated serum IL-6 levels in obesity are not reflected in the CNS, at least not in the cerebrospinal fluid, where a surprising reduction of the IL-6 peptide is revealed in overweight and obese men (Stenlöf et al., 2003). These data also suggest that the function of peripheral and CNS IL-6 is likely divergent. The neural circuits and mechanisms engaged by CNS-produced IL-6 to reduce body weight and body fat and their role in obesity are poorly understood.

To determine whether brain IL-6 production is affected by high-fat diet (HFD)-induced obesity, and to narrow the sites of
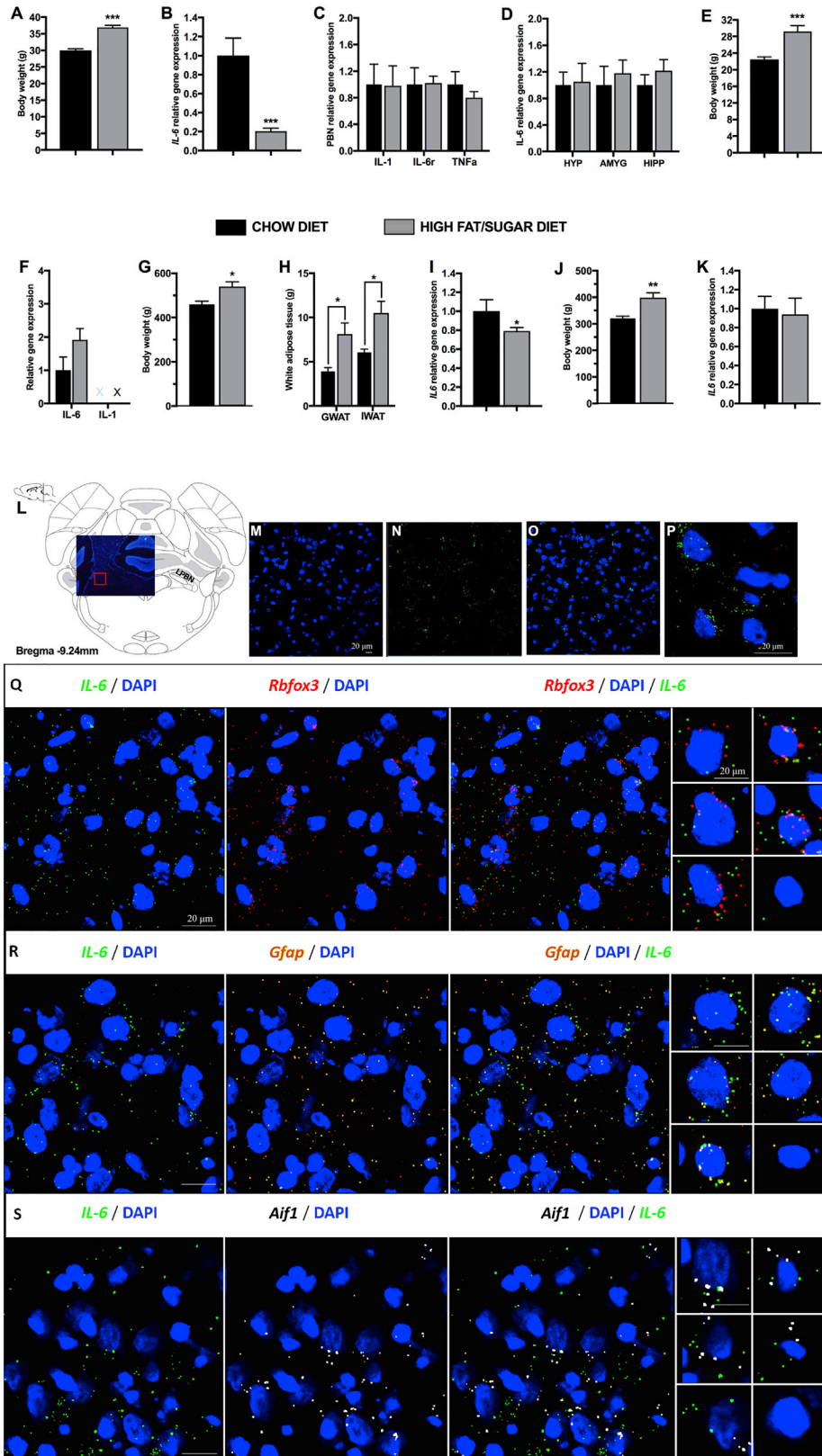
(legend on next page)

potential interest for the weight- and the fat-controlling role of IL-6, we initially evaluated IL-6 gene expression in key energy balance-controlling brain regions in obese male and female mice. Surprisingly, a very strong reduction in IL-6 gene expression in HFD-fed mice was only detected in one brain nucleus—the parabrachial nucleus (PBN)—but not in the hypothalamus. This was an unexpected finding, because most studies to date only evaluate the hypothalamus as the main neural substrate for the weight loss effects of IL-6 (Benrick et al., 2009; Le Foll et al., 2015; Schéle et al., 2012; Timper et al., 2017).

While the lateral PBN (lPBN) is a brain nucleus that received much less attention for its role in food intake and energy expenditure control compared to the hypothalamus, we and others have previously demonstrated that it receives energy-balance-relevant anorexigenic inputs from, e.g., leptin, GLP-1, and melanocortin (Alhadeff et al., 2014a, 2014b; Flak et al., 2014; Richard et al., 2014; Shah et al., 2014). Indirect activation of lPBN results in severe anorexia in mice indicating a powerful position of this nucleus in feeding control (Wu et al., 2009).

Using genetic, molecular, and pharmacological manipulations, the lPBN was evaluated as a potential previously unknown, but critical site of, the anorexic action of IL-6, capable of producing and responding to IL-6, in a sex-specific manner, in obesity. Utilizing a recently developed retrograde neuronal tracing strategy, we assessed lPBN as a potential source of IL-6 to the hypothalamus. Moreover, the ability of lPBN IL-6 to control thermogenesis, both via neural and hormonal mechanisms, was determined. Since IL-6 was previously shown to enhance intracellular signaling induced by the anorexic adipose hormone, leptin, in the hypothalamus (Larsen et al., 2016; Le Foll et al., 2015), we assessed the cooperative interaction of IL-6 and leptin in feeding and thermogenesis at the level of the lPBN. Finally, we determined whether thermogenic contexts other than obesity, namely, cold exposure and stress, affect lPBN IL-6.

RESULTS

Potently Reduced IL-6 Expression in the PBN of Obese Male Mice and Rats

How CNS IL-6 production is affected by obesity is poorly understood; thus, we investigated the effect of HFD exposure on IL-6 gene expression in the PBN. For both mice and rats, the choice of an obesogenic diet was based on in-house testing designed to find the most effective diet at inducing hyperphagia and obesity in each species. As a result, mice were fed regular chow (Global Diet #2016; Harlan-Teklad; 4% kcal from fat) or HFD (catalog #D12492; Research Diets; 60% kcal from fat) previously shown to increase visceral fat, produce hyperinsulinemia, and insulin resistance after an 8-week exposure (Della Vedova et al., 2016; Lin et al., 2000). Male or female Sprague-Dawley CD rats were offered chow and water or exposed to a high-fat/high-sugar diet consisting of *ad libitum* access to chow, or lard and sucrose (50%/50% mix), and water (Diepenbroek et al., 2017). Eight weeks of HFD feeding increased the body weight of male ($p < 0.001$, Figure 1A) and female mice (Figure 1E). The mRNA levels of PBN IL-6 were significantly reduced in male ($p < 0.0001$, Figure 1B), but not in female, mice (Figure 1F). To clarify whether these changes coexisted with general inflammatory markers, we assessed the PBN gene expression of IL-1 and tumor necrosis factor alpha (TNF-α), two classic inflammatory markers. Their expression, in contrast to IL-6, was not altered in diet-obese mice (Figure 1C, males; Figure 1F, females). Further, IL-6 levels were unaltered in other food intake-associated regions, such as hypothalamus, amygdala, and hippocampus (Figure 1D), suggesting that decrease in *Il-6* mRNA levels was not a global response to HFD diets. Next, we investigated whether the obesity-associated reduction in PBN IL-6 expression, detected in male mice, also occurs in male rats. As

---

Figure 1. Interaction of IL-6 Gene Expression with Sex and Diet in the Parabrachial Nucleus

(A–F) Mice, 5 weeks old at the start of the experiment, were fed a normal chow or a high-fat diet for 8 weeks. Measurements shown were taken at 8 weeks on the respective diet.

(A) Body weight of male mice at 13 weeks of age (n = 10, for all groups).

(B) IL-6 gene expression in male mice in the parabrachial nucleus as detected by qPCR.

(C) Expression of other inflammation-associated genes (n = 8–9) in male mice in the parabrachial nucleus as detected by qPCR.

(D) qPCR of IL-6 expression in other food intake-associated brain regions in male mice, hypothalamus (HYP), amygdala (AMYG), and hippocampus (HIPP) (n = 6–10).

(E) Body weight of female mice at 13 weeks old (n = 10, for all groups).

(F) qPCR of IL-6 and IL-1 gene expression in the parabrachial nucleus of female mice. IL-1 was below the detection threshold.

(G) Body weight of male rats on a high-fat/high-sugar diet (n = 5).

(H) White adipose tissue mass in male rats on a chow or a high fat/high-sugar diet.

(I) IL-6 gene expression, as detected by qPCR, in male rats maintained on a chow or a high-fat/high-sugar diet, 14 weeks on the tissue collection day.

(J and K) Body weight (J) and IL-6 expression (K) in female rats maintained on a chow or a high-fat/high-sugar diet for 14 weeks.

(L–S) IL-6 mRNA is displayed in green, and cell nuclei is displayed in blue (DAPI).

(L) Lateral parabrachial nucleus IL-6 mRNA was detected using fluorescent *in situ* hybridization (RNAScope).

(M–P) DAPI (M), IL-6 (N), DAPI with IL-6 (O), and a high-resolution image of single cells in the lPBN showing IL-6 and DAPI (P).

(Q–S) To understand the cellular origin of IL-6 in the lPBN, we used RNAScope to co-localize IL-6 mRNA with neuronal (Rbfox3; red; Q), glial (GFAP; orange; R), or microglial (AIF1; gray; S) mRNA markers. Gene expression data were normalized to the housekeeping gene *Ppia* and are presented as mean ± SEM. PBN, parabrachial nucleus; *Il-6*, interleukin-6; *Il-1*, interleukin-1; *Il-6r*, IL-6 receptor; *Tnf-α*, tumor necrosis factor alpha; GWAT, gonadal white adipose tissue; IWAT, inguinal white adipose tissue; X, cycle threshold values in real-time PCR were out of the defined threshold point of 40 cycles, indicating that IL-1 levels were too low to be evaluated and compared.

For comparison of male and female IL-6 gene expression, see Figure S1. For results of approximate quantification of co-expression of each of the cellular markers with IL-6 mRNA, see Figure S2. All gene expression presented here as bar graphs was detected by real-time qPCR. Data represent mean ± SEM. *p < 0.05; **p < 0.005; ***p < 0.001; compared with respective controls, unpaired Student's t test comparisons.
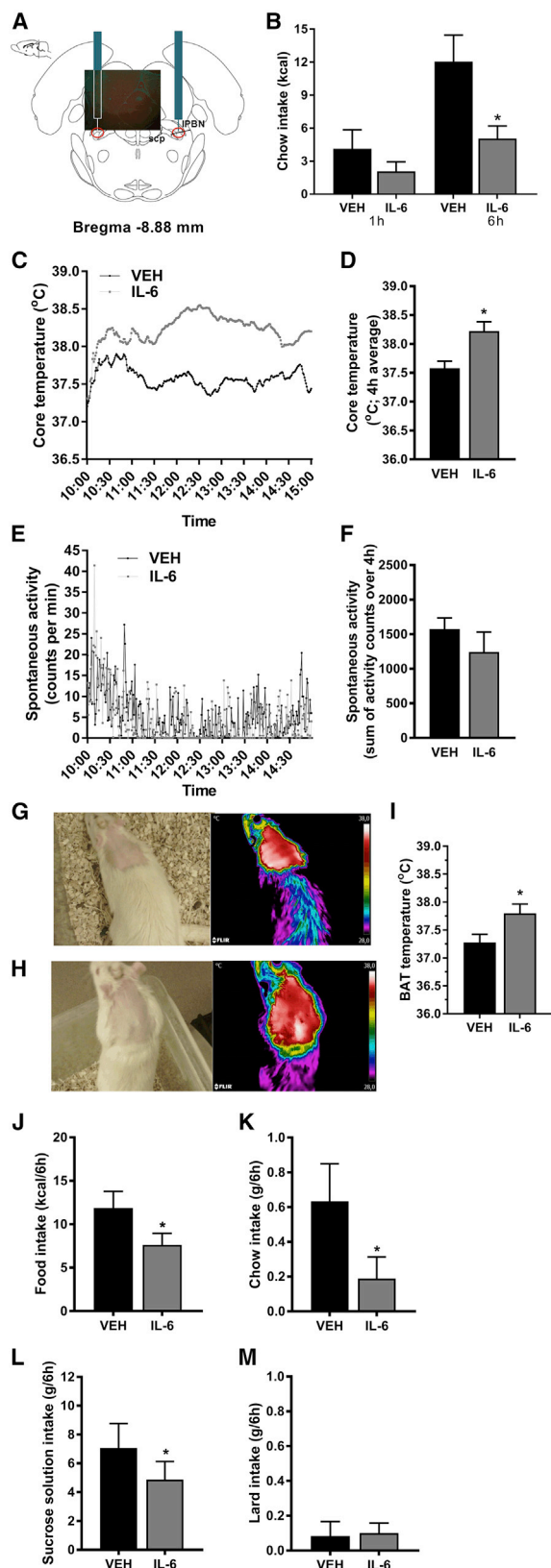
Figure 2. IL-6 Acts in the IPBN to Reduce Food Intake and Increase Thermogenesis

(A) Representative confocal image of the injection site pasted into the corresponding rat brain atlas section is displayed.

(B–M) IL-6 or vehicle control was microinjected in the IPBN of male rats.

(B) Chow intake was measured 1 h and 6 h post-injection.

(C) Core temperature was measured every minute for 5 h post-injection. Injections were performed at 10.00.

(D) Core temperature averaged over 4 h starting immediately post-injection.

(E) Spontaneous activity was measured for 5 h post-injection. Injections were performed at 10.00.

(F) Cumulative spontaneous locomotor activity over 4 h.

(G and H) Representative images of rat infrared thermographic pictures used to assess BAT temperature after vehicle (G) and IL-6 injection (H).

(I) BAT temperature was measured 4 h–5 h post-IL-6 microinjections into the IPBN in another cohort of rats and compared to controls.

(J–M) Intra-IPBN IL-6 was injected in another cohort of rats fed a high-fat/high-sugar-fed diet for 3 weeks at the time of testing and food intake expressed as total calories consumed (J), chow intake (K), sucrose solution intake (L), and lard intake (M) were measured 6 h post-IL-6 microinjections. BAT, brown adipose tissue; IPBN, lateral parabrachial nucleus; IL-6, interleukin-6; VEH, artificial cerebrospinal fluid.

Data represent mean ± SEM. *$p < 0.05$, paired comparisons Student's t test. n = 5–9.

expected, the high-fat/high-sugar diet-fed rats gained significantly more weight than did controls ($p < 0.05$, Figure 1G) and significantly more gonadal and inguinal white adipose tissue (GWAT and IWAT) ($p < 0.05$, Figure 1H). Most importantly, they had reduced levels of *Il-6* mRNA in the PBN ($p < 0.05$, Figure 1I). Female rats, on the other hand, followed the same pattern as female mice and did not show any significant reduction in PBN IL-6 expression (Figure 1K), despite a significant weight gain (Figure 1J).

In the IPBN, Neurons, Astrocytes, and Microglia Contain IL-6 mRNA

In situ fluorescent hybridization indicated the clear presence of IL-6 mRNA throughout IPBN (Figures 1L–1P). Outside of the IPBN or in cell cultures, neurons, astrocytes, and microglia are capable of producing IL-6 in response to gut-brain signals (Hidalgo et al., 2010; Le Foll et al., 2015; López-Ferreras et al., 2018; Shirazi et al., 2013); which cell type produces IL-6 in the IPBN is unknown. As indicated in Figure 1, *Il-6* mRNA was found to be co-expressed with neuronal (Rbfox3; Figure 1Q), glial (GFAP; Figure 1R), and microglial (Aif1; Figure 1S) mRNA, indicating that IL-6 can be produced by all three cell types. Approximate quantification of the co-expression of IL-6 with the three marker mRNAs indicated that neurons are the major source of IL-6 in the IPBN, followed by astrocytes and microglia (Figure S2).

IL-6 Acts in the IPBN to Reduce Food Intake and Increase Body Temperature

We investigated whether IL-6 plays a role in regulating body weight or energy expenditure through actions in the IPBN. IL-6 IPBN microinjection led to a significant reduction in chow intake 6 h after injection (Figure 2B). Lateral PBN-injected IL-6 also produced hyperthermia ($p < 0.05$, Figures 2C and 2D) without affecting spontaneous home-cage activity ($p > 0.05$, Figures 2E and 2F). Thermal imaging revealed
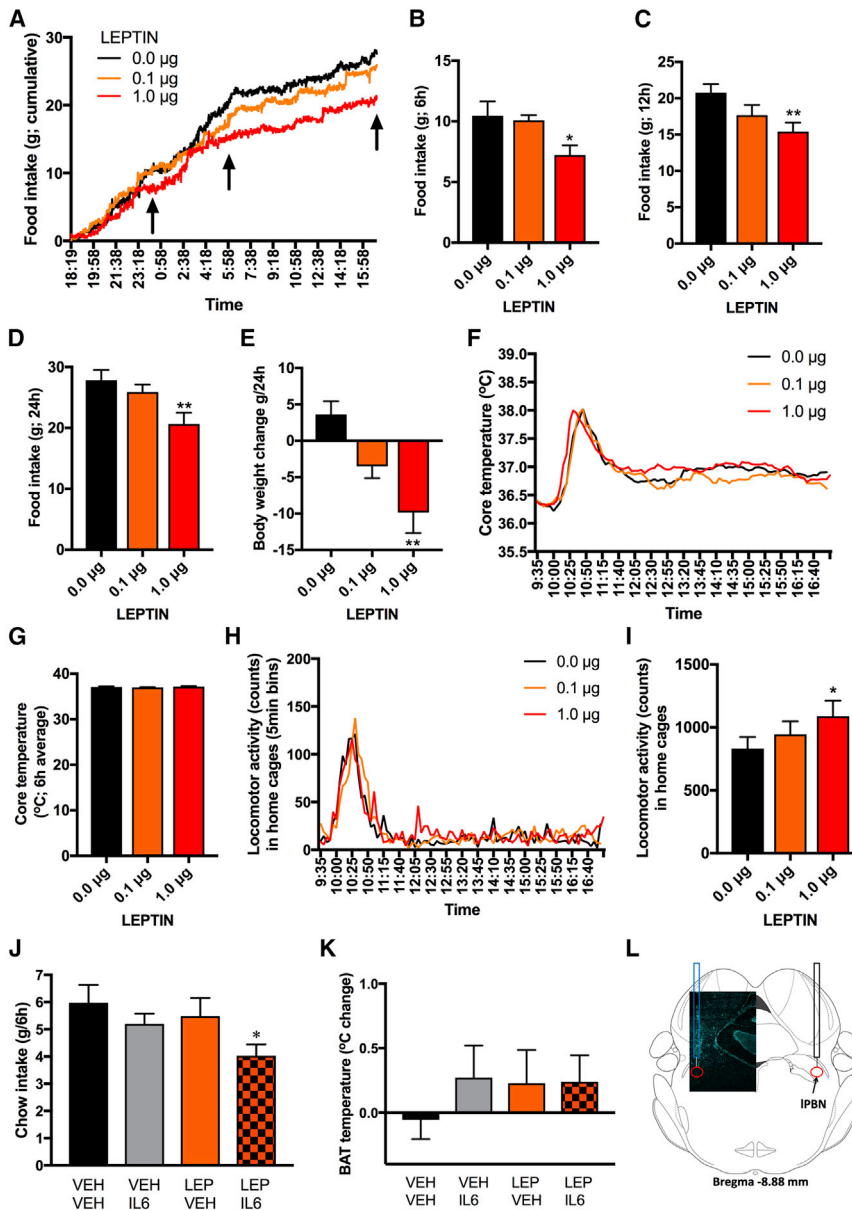
Figure 3. Cooperative Interaction of Leptin and IL-6 at the Level of the lPBN

(A–I) Leptin was microinjected into the lPBN of 11-week-old male rats.

(A) Chow intake was continuously measured (minute by minute) immediately starting after injections as displayed on the line graph (n = 6).

(B–D) Cumulative chow intake at the following time points: 6 h (B), 12 h (C), and 24 h (D), as indicated with black arrows on the line graph.

(E) Body weight 24 h post-lPBN leptin microinjections.

(F) Core body temperature was telemetrically collected every 5 min in another group of rats (n = 18) microinjected with leptin into the lPBN.

(G) Core temperature is averaged over the 6 h post-injection time period.

(H) Spontaneous home-cage locomotor activity was telemetrically collected (n = 18) in rats microinjected with leptin into the lPBN.

(I) Sum of all post-injection locomotor counts accumulated for 6 h post-injections.

(J and K) In a new cohort of 11-week-old male rats (n = 12) chow intake and BAT temperature were measured after intra-lPBN delivery of sub-threshold doses of IL-6 (0.1 μg) or leptin (0.1 μg) alone, or delivery of the two substances together into the lPBN. (J) Cumulative chow intake collected over 6 h post-injections. (K) BAT temperature measured with infrared thermography displayed as temperature change from pre-injection baseline to 4–5 h after injections (n = 12).

(L) Representative confocal image of a cannula tract in lPBN. lPBN, lateral parabrachial nucleus; IL-6, interleukin-6; BAT, brown adipose tissue.
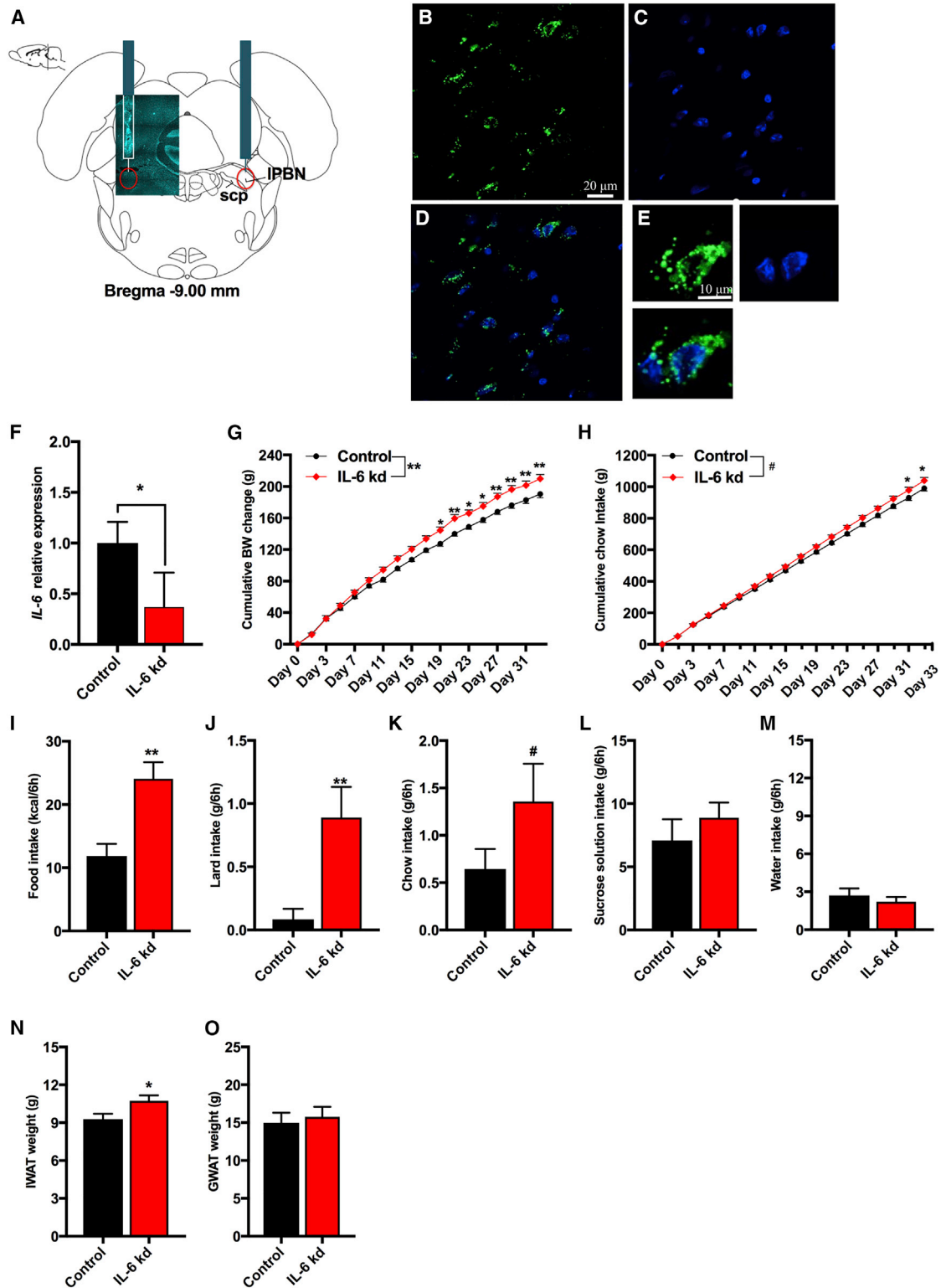
For intra-lPBN effect of leptin on heart rate, see Figure S3, and for effect of the combination of leptin and IL-6 on 24-h chow intake, see Figure S4, and on tail temperature, see Figure S5. Data represent mean ± SEM. *p < 0.05; **p < 0.01; two-way ANOVA (J and K) and one-way ANOVA (B–E, G, and I) were used for comparisons with Sidak's post hoc test.

that IL-6 lPBN treatment increased brown adipose tissue (BAT) temperature (p < 0.05, Figure 2I, representative images: Figures 2G and 2H). Notably, the hypophagic effect of IL-6 in the lPBN persisted under obesogenic diet feeding conditions (p < 0.05, Figure 2J). Chow and sugar solution intakes were significantly decreased (p < 0.05, Figures 2K and 2L), whereas lard intake was unaffected (Figure 2M). The caloric intake of chow and high-fat/high-sugar diet-fed rats injected with IL-6 was 55% and 78% of the vehicle group for chow and high-fat/high-sugar diet-fed rats respectively. Even though it appears that the intake reduction was less effective under the high-fat/high-sugar diet-fed condition, this difference did not reach statistical significance (p = 0.3). Alternatively, because we offered chow, sucrose, and lard separately, and the intake of chow was potently reduced, while the intake of lard was not altered, lPBN IL-6 may be more effective at reducing intake of specific macronutrients (Bodnar, 2018; Myers, 2018; Sclafani, 2016; Sclafani and Ackroff, 2016).

Leptin Acts in the lPBN to Alter Food Intake, but Not Body Temperature

Leptin receptor is expressed in the PBN of mice and rats (Elmquist et al., 1998; Grill et al., 2002) and phosphorylation of STAT3 can be induced in the lPBN by peripheral leptin administration (Hosoi et al., 2002). The leptin receptor partly shares downstream signaling (including pSTAT3) with IL-6Rα (Dunn-Meynell et al., 2016). Leptin and IL-6 are related structurally, and both ligands produce anorexia by acting on the lPBN. Leptin, microinjected in the lPBN suppressed food intake when applied at the start of the dark cycle (active period) or during the mid-light cycle (inactive period) (Figures 3A, S3C, and

Figure 4. Disrupted Feeding and Body Weight Control in lPBN IL-6 Knockdown

(A) Representative image of rat coronal brain atlas drawing and male rat tissue section showing lPBN-targeted AAV infusions.

(B–E) GFP expression (B), DAPI (C), and the two signals together showing AAV infection (D) in the lPBN cells. High-resolution DAPI (in cyan: A; in blue: C–E).

S3D), data in line with one previous report (Alhadeff et al., 2014b). Cumulative chow intake was decreased at 6 h ($F_{(2, 10)} = 5.496$, $p < 0.05$; Figure 3B), 12 h ($F_{(2, 10)} = 6.685$, $p < 0.05$; Figure 3C), and 24 h ($F_{(2, 10)} = 7.464$, $p < 0.05$; Figure 3D) time points, leading to a decreased body weight measured at 24 h ($F_{(2, 12)} = 7.55$, $p < 0.01$; Figure 3E). In contrast to IL-6, core body temperature was not altered by lPBN leptin treatment ($F_{(2, 34)} = 1.765$, $p > 0.05$; Figures 3F and 3G), and spontaneous locomotor activity was increased (Figures 3H and 3I; $F_{(2, 34)} = 3.493$, $p < 0.05$). Leptin treatment did not affect heart rate (Figures S3A and S3B). This is in contrast to leptin's effect in the NTS, where both body temperature and heart rate are clearly increased by the same doses of leptin as those applied here in the lPBN (Skibicka and Grill, 2009).

Cooperative Interaction of Leptin and IL-6 on Food Intake Control

Since both leptin and IL-6 produce an anorexic response by acting on their receptors in the lPBN, we hypothesized an interactive relationship between these two signals at the level of the lPBN. Leptin and IL-6 (both at 0.1 μg) did not affect food intake, activity, or core temperature, and thus these ligand doses were labeled as subthreshold and used to test for a cooperative interaction between these two signals. Results indicated that IL-6 and leptin indeed interact to suppress food intake (two-way ANOVA: IL-6 alone: $F_{(1, 11)} = 0.21$, $p > 0.05$; leptin alone $F_{(1, 11)} = 0.88$, $p > 0.05$; interaction IL-6 × leptin $F_{(1, 11)} = 0.563$, $p = 0.05$; Figure 3J). This suppression of chow intake did not persist at 24 h (Figure S4). BAT region temperature was unaffected (IL-6 alone: $F_{(1, 11)} = 4.524$, $p > 0.05$; leptin alone $F_{(1, 11)} = 7.652$, $p < 0.05$; interaction IL-6 × leptin $F_{(1, 11)} = 1.528$, $p > 0.05$; Figure 3K). Tail-surface temperature was also unaffected by IL-6, leptin, or the combination treatment (Figure S5). These results suggest that leptin and IL-6 can acutely act in concert, possibly by sharing a common downstream target, ultimately amplifying each other's reduction of food intake. The shared downstream signaling is likely to include phosphorylation of STAT3, at least previous data indicate that ventromedial hypothalamic leptin signaling is enhanced by induction of IL-6, which then interacts with its receptors to activate STAT3 signaling and gene transcription downstream of the leptin receptor (Le Foll et al., 2015). Moreover, we have previously shown that both IL-6 and leptin, delivered intracerebroventricularly, induce pSTAT3 in the arcuate nucleus (Anesten et al., 2017).

Reduction in lPBN IL-6 Leads to Weight and Fat Gain along with Increased Food Intake

Because we found *Il-6* mRNA in the lPBN, along with a modulatory effect of IL-6 injections in this area on food intake and core body temperature, we next set out to determine the physiological role of IL-6 in lPBN by evaluating the impact of chronic, genetic lPBN IL-6 reduction. Adeno-associated virus (AAV)-small interfering RNA (siRNA) targeting *Il-6* mRNA, injected into the lPBN (representative images of the injection: Figures 4A–4E), efficiently and specifically reduced *Il-6* mRNA in the lPBN ($p < 0.05$; Figure 4F), but not in other brain areas (e.g., PVH: relative delta Ct value of scrambled controls was 12.52 vs. 12.88 of IL-6 knockdown [KD]). The lPBN IL-6 KD increased body weight gain (two-way ANOVA, interaction $F_{(17, 544)} = 8.345$, $p < 0.01$ and treatment effect $F_{(1, 32)} = 7.548$, $p < 0.05$; Figure 4G) and food intake (two-way ANOVA: interaction $F_{(17, 544)} = 4.944$, $p < 0.01$; treatment $F_{(1, 32)} = 3.462$, $p > 0.05$; Figure 4H) in chow-fed rats. The onset of increased food intake in lPBN IL-6 KD group ($p < 0.05$) was observed 12 days following increased weight gain. In high-fat/high-sugar diet-fed rats, the total amount of calories consumed over 6 h in the light period was significantly increased by lPBN IL-6 KD ($p < 0.01$, Figure 4I), with lard ($p < 0.05$, Figure 4J) and chow ($p = 0.07$, Figure 4K), largely driving the increased intake, while sucrose intake remained unaffected ($p > 0.05$, Figure 4L). Water intake was not altered by the lPBN IL-6 reduction ($p > 0.05$, Figure 4M). The increased weight gain was also associated with increased mass of the subcutaneous IWAT ($p < 0.05$, Figure 4N). The weight of GWAT was not altered ($p > 0.05$, Figure 4O) by the treatment. The weight gain and long-term hyperphagia driven by lPBN IL-6 reduction were not detected in two separate cohorts of rats fed two different obesogenic diets (Figures S6 and S7) as maintenance diets; observation previously reported for IL-6−/− mice (Matthews et al., 2010).

PBN IL-6 Knockdown Lowers Core Body Temperature

Changes in body weight after lPBN IL-6 KD emerged prior to the changes in food intake; therefore, we posited that IL-6 KD reduced energy expenditure. Since intra lPBN IL-6 delivery increased core body temperature (Figures 2C and 2D), we hypothesized that lower energy expenditure results from lower levels of thermogenesis in the IL-6 KD rats. Telemetric monitoring of home-cage core body temperature and activity in lPBN IL-6 KD rats and controls (Figures 5A–5D) indicated that, in line with our hypothesis, core body temperature was significantly lower ($p < 0.01$, Figure 5B) in lPBN IL-6 KD rats when compared to controls. The difference in core body temperature

---

(F) IL-6 gene expression as detected by qPCR in control rats and rats with siRNA-mediated knockdown of IL-6 gene (n = 9–12).

(G) Cumulative body weight gain of the IL-6 KD group compared to controls (n = 17 for all groups). Day 0 represents the day of siRNA introduction.

(H) Cumulative chow intake in the same rats.

(I–M) Acute light cycle measurements over a period of 6 h of total caloric intake (I), intake of lard (J), intake of chow (K), intake of sucrose (L), and intake of water (M) in male rats maintained on a high-fat/high-sugar diet for 3 weeks.

(N) Inguinal white adipose tissue of IL-6 KD (n = 17) in comparison to controls (n = 17).

(O) Gonadal white adipose tissue mass in the same rats.

For daily chronic intake on two different obesogenic diets, see Figures S6 and S7. The n = 17 reflects data combined from two independent experiments/cohorts of rats. IL-6 KD, interleukin-6 knockdown; lPBN, lateral parabrachial nucleus; scp, superior cerebellar peduncle; IWAT, inguinal white adipose tissue; GWAT, gonadal white adipose tissue. Data represent mean ± SEM. *$p < 0.05$; **$p < 0.01$; #$p = 0.07$. Two-way ANOVA, followed by Sidak's post hoc test, or unpaired Student's t test when appropriate.
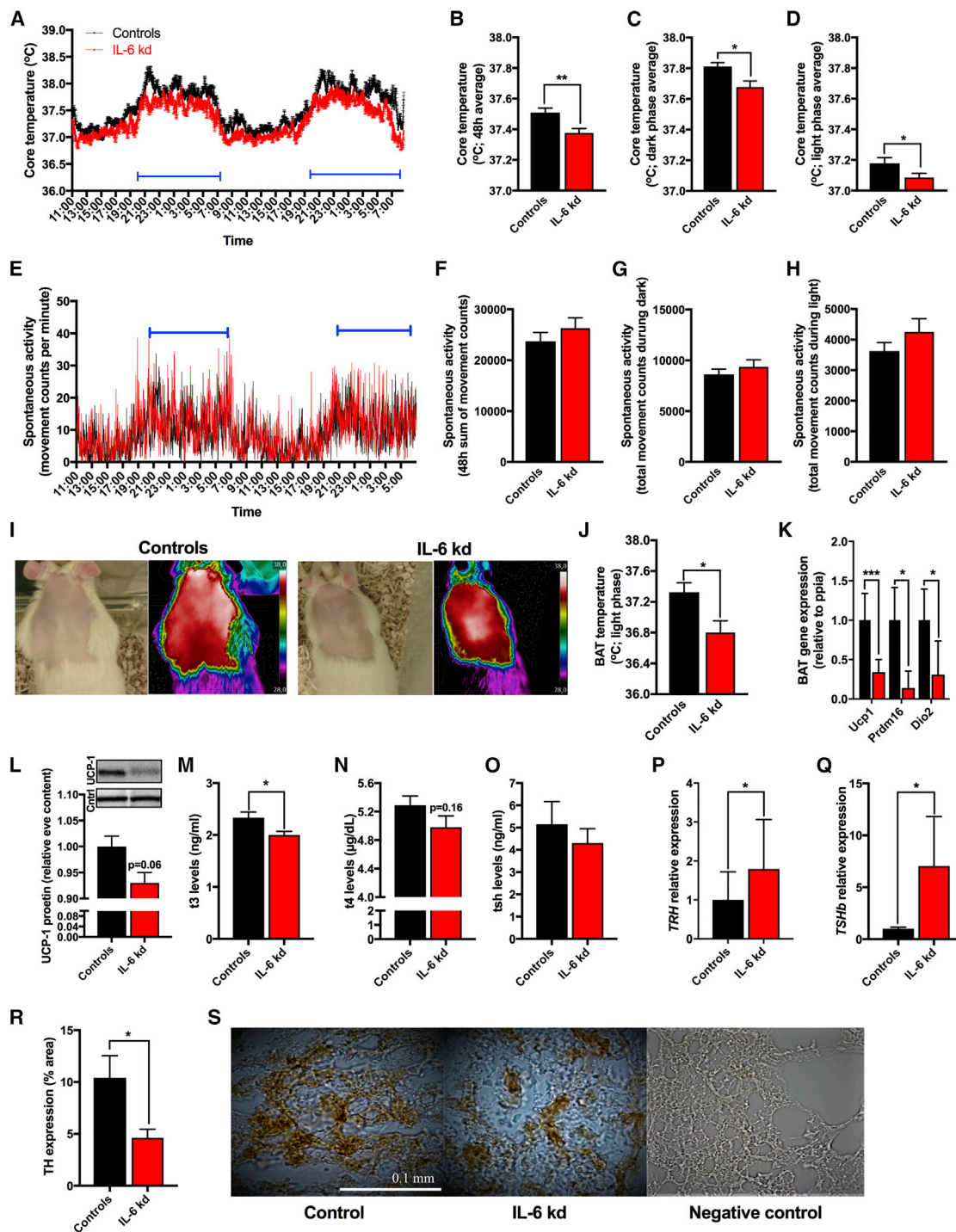
Figure 5. Mechanisms Underlying Disrupted Thermogenesis in lPBN IL-6 Knockdown

(A–S) Virally introduced siRNA, designed to knockdown IL-6 gene expression, was delivered into the lPBN, as shown in Figure 4, and all thermogenic and locomotor testing was conducted in male rats 5–6 weeks after siRNA introduction. All tissue and plasma samples were collected from the same rats 6 weeks later.

(A) Core body temperature was telemetrically collected every minute for 48 h (n = 8 each in control and IL-6 KD group).

(B) 48-h average of all collected core temperature values.

(C) Average core temperature of two consecutive dark phases.

(D) Average core temperature from two consecutive light phases.

(E) Spontaneous activity collected every minute for 48 h.

(F) 48-h sum of all collected spontaneous activity values.

(legend continued on next page)

was present in both the light and dark cycle phases (p < 0.05, Figures 5C and 5D). During the same data collection period home-cage activity was not altered (Figures 5E–5H), eliminating hyperlocomotion as the source of increased energy expenditure and increased body temperature.

PBN IL-6 Knockdown Decreases BAT Thermogenic Activity

To understand the mechanisms underlying the reduction in body temperature, BAT thermogenesis was evaluated using infrared thermography (representative images presented in Figure 5I) and revealed that lPBN IL-6 KD rats had lower BAT temperature (p < 0.05, Figure 5J). Consistent with these results, gene expression levels of thermogenesis permissive mitochondrial uncoupling protein 1 (*Ucp1*) (Cannon and Nedergaard, 2004; Ulrich-Lai et al., 2011) were significantly reduced (p < 0.001, Figure 5K) after IL-6 KD. PR domain zinc-finger protein 16 *(Prdm16)*, a transcription factor recently demonstrated to be required in young mice to suppress the expression of white-fat-selective genes in BAT (Harms et al., 2014), was also reduced in rats with reduced lPBN IL-6 *(*p < 0.05, Figure 5K). Type II deiodinase *(Dio2)*, an enzyme responsible for conversion of the low-activity form thyroxine (T4) to the active form 3, 3′, 5-triiodothryonine (T3), gene expression was also reduced in lPBN IL-6 KD rats, (p < 0.05, Figure 5K). Moreover, a strong trend (p = 0.06) indicated reduced UCP-1 protein in BAT (Figure 5L).

PBN IL-6 Knockdown Decreases Plasma Thyroid Hormone Levels and BAT Sympathetic Activity

Next, we examined whether changes in hormonal (thyroid axis) and neural (SNS innervation) CNS outputs underlie reduced BAT thermogenesis detected in lPBN IL-6 KD rats. To determine whether the hypothalamus-pituitary-thyroid axis is affected by the lPBN IL-6 manipulation, we measured blood plasma levels of T3, T4, and thyroid-stimulating hormone (TSH). Results revealed a significant reduction of T3 in lPBN IL-6 KD rats compared to controls (p < 0.05, Figure 5M), with no significant changes detected in the levels of T4 (p = 0.16, Figure 5N) or TSH (p > 0.05, Figure 5O). *TRH* gene expression in the hypothal-

amus (p < 0.05, Figure 5P) and *TSHb* expression in pituitary (p < 0.05, Figure 5Q) were increased by the KD. BAT UCP1 levels can be increased by activation of the sympathetic innervation to BAT (Cannon and Nedergaard, 2004) or elevated T3 (Bianco and Silva, 1987a, 1987b; Obregon, 2014). Therefore, to understand whether the decreased BAT activity is associated with a reduced sympathetic output to this tissue, we quantified BAT TH protein expression, the rate-limiting enzyme in norepinephrine production. TH protein in BAT of lPBN IL-6 KD rats was robustly reduced (p < 0.05, Figure 5R), consistent with reduced sympathetic output to the BAT of lPBN IL-6 KD rats.

Anxiety-like Behavior in lPBN IL-6 Loss

Central IL-6 is linked to stress-related disorders, such as depression and anxiety (Erta et al., 2015; Hodes et al., 2016), and the lPBN has well-established neuroanatomical links to emotionality regulating regions, such as the amygdala (Bernard et al., 1996; Gauriau and Bernard, 2002). Therefore, we evaluated the potential impact of IL-6 loss in the lPBN on anxiety-like behavior using two well-validated rodent tests of anxiety: the open field and the elevated plus maze (EPM). Lateral PBN IL-6 KD rats spent less time in center area during the open-field test (p < 0.05, Figure 6A) and more time in the periphery (p < 0.05, Figure 6B), which may be indicative of increased anxiety-like behavior. However, the IL-6 KD rats also displayed lower locomotor activity during this test (p < 0.01, Figure 6C), suggesting that changes in locomotor activity may be a competing explanation for the open-field test results. This idea was further supported by the lack of significant effect on time spent in open arms of the EPM (p > 0.05, Figure 6D). Also, during the EPM test the rats with reduced lPBN IL-6 moved significantly less compared to control rats (p < 0.05, Figure 6E). Thus, the open field and EPM results may indicate a lower locomotor activity in a novel environment in IL-6 KD. *Crh* gene expression in the PVH was not altered (Figure 6F).

lPBN IL-6 Is Unaffected by Acute Stress

Because locomotor activity of the IL-6 KD rats was reduced only during exposure to a novel environment and not in the homecage environment, we hypothesized an interaction of lPBN IL-6 with

(G) Sum of activity from two consecutive dark phases.

(H) Sum of activity from two consecutive light phases.

(I) Representative images of infrared thermography of BAT region in control and IL-6 KD.

(J) BAT temperature as detected by infrared thermography during the light phase (n = 8 and 9, control and IL-6 KD, respectively).

(K) BAT gene expression, as detected by qPCR, of the following genes: *UCP1*, thermogenesis permissive mitochondrial protein; *PRDM16*, a transcription factor required for suppression of white-fat-selective genes in BAT and *DIO2*, an enzyme responsible for conversion of the low-activity form thyroxine (T4) to the active form 3, 3′, 5-triiodothryonine (T3). *Ucp1*, uncoupling protein 1; *Prdm16*, PR domain zinc-finger protein 16; *Dio2*, type II deiodinase.

(L) UCP-1 protein levels in BAT in the IL-6 KD rats compared to control rats (n = 8 each). Image above the graph shows the representative western blot bands for each treatment group.

(M) Plasma T3 levels in IL-6 KD rats and controls (n = 8, each).

(N) Plasma T4 levels.

(O) Plasma TSH levels.

(P) TRH gene expression in the hypothalamus as detected by qPCR (n = 5, each).

(Q) TSHb expression in the pituitary (n = 5, each) as detected by qPCR.

(R) Quantification of TH protein expression in BAT tissue (n = 12).

(S) Representative images of *TH* expression (shown in brown) in BAT of controls and IL-6 KD, along with a negative control. TSHb, thyroid-stimulating hormone beta subunit; TRH, thyroxine-releasing hormone; BAT, brown adipose tissue; TH, tyrosine hydroxylase.

The results presented here were derived from tissues of rats with physiology and metabolism assessed and displayed in Figure 4. All gene expression presented here as bar graphs was detected by real-time qPCR. Data represent mean ± SEM. *p < 0.05; **p < 0.01; ***p < 0.001; unpaired Student's t test comparisons.
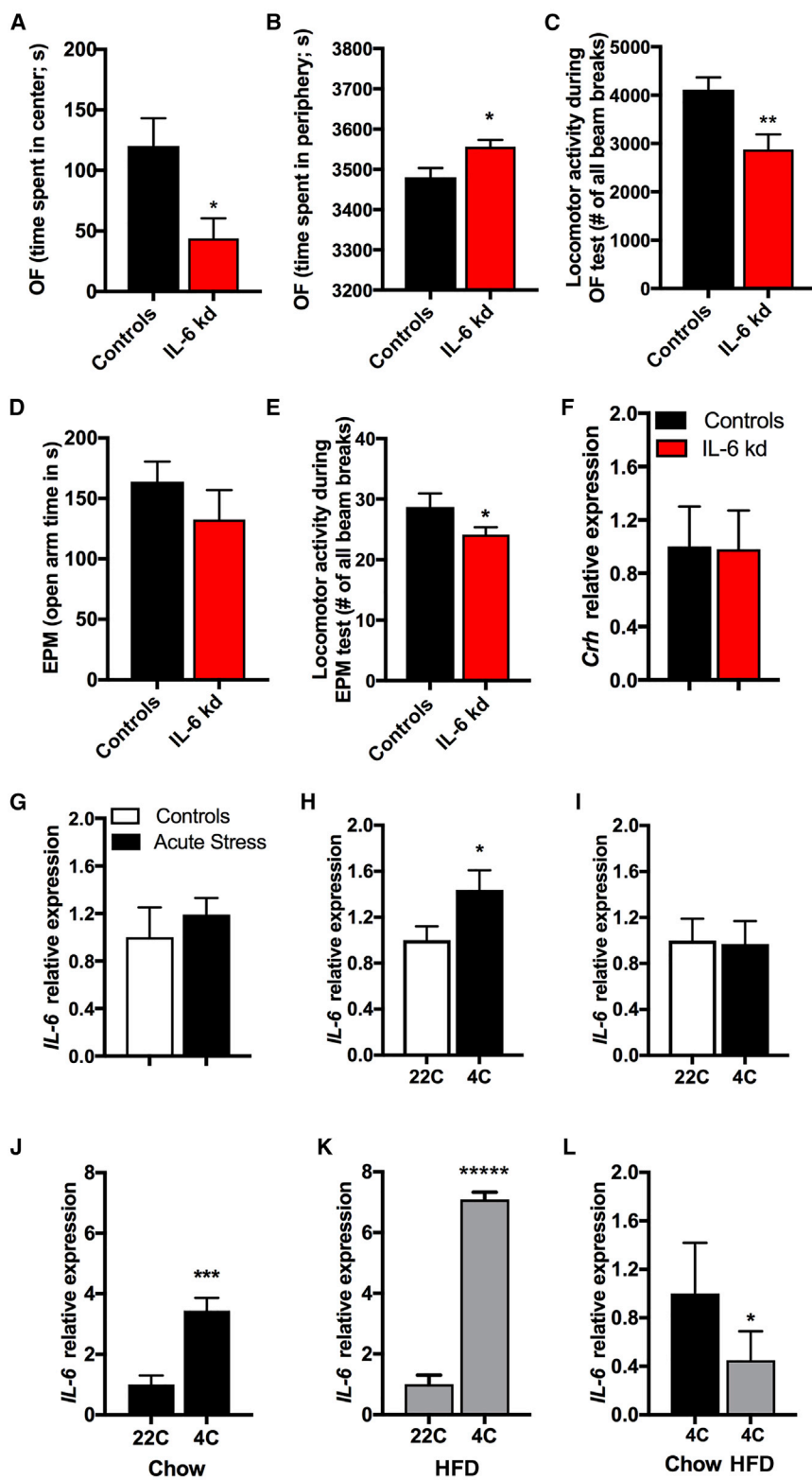
Figure 6. Physiological Contexts Interacting with lPBN IL-6

(A–F) Virally introduced siRNA, designed to knockdown IL-6 gene expression, was delivered into the lPBN, as shown in Figure 4, and anxiety-like behavior and concurrent locomotor activity testing was conducted in male rats 7 weeks after siRNA introduction.

(A) Time spent in the center of an open-field arena (n = 7–8).

(B) Time spent in the periphery of the open-field arena.

(C) Total locomotor activity of IL-6 KD rats in comparison to controls.

(D) Time in the open arms of the elevated plus maze (EPM) of IL-6 KD rats in comparison to control rats.

(E) Total locomotor activity of IL-6 KD and controls.

(F) Expression of *Crh* in the hypothalamus, as detected by qPCR, in IL-6 KD and control rats.

(G) Gene expression levels of IL-6, as detected by qPCR, in PBN of 11-week-old chow-fed rats challenged with a 30-min acute-restraint stress (n = 7–8).

(H and I) PBN IL-6 mRNA expression after 48-h exposure to ambient cold in 11-week-old chow-fed male (n = 6 per treatment group) (H) and female (n = 7 per treatment group) rats (all from another new cohort) (I).

(J–L) A new cohort of male mice, fed a high-fat diet for 8 weeks prior to testing, and 13 weeks old at the time of testing, was exposed to cold for 48 h, and brain tissues were immediately collected after cold exposure for testing IL-6 mRNA levels in the PBN of (J) chow- and (K) HFD-fed mice (n = 6–10). Comparison of IL-6 levels in the PBN of cold-exposed chow- and HFD-fed mice (L).

All gene expression presented here as bar graphs was detected by real-time qPCR. Data represent mean ± SEM. *$p < 0.05$; **$p < 0.01$; ***$p < 0.001$; *****$p < 0.00001$; unpaired Student's t test comparisons. OF, open field.

in lPBN. We found that, contrary to our hypothesis, acute stress (30-min restraint) did not affect IL-6 gene expression levels in the lPBN ($p > 0.05$, Figure 6G).

lPBN IL-6 Sensitivity to Ambient Cold Exposure

Because we found a clear role of lPBN IL-6 in BAT thermogenesis, and cold exposure engages the CNS in order to increase BAT thermogenesis, we hypothesized that cold exposure will increase lPBN IL-6 levels. Indeed, IL-6 gene expression in the lPBN was increased by 50% in male rats exposed to 4°C cold for 48 h ($p < 0.05$, Figure 6H). Gene expression of IL-6 in the lPBN of female rats was unaltered by ambient cold (Figure 6I). Additionally, chow and HFD-fed mice were exposed to 4°C cold for 48 h, and IL-6 gene expression in the lPBN was measured at

stress. Accordingly, to further pinpoint the physiological/patho-physiological conditions that affect lPBN IL-6, we evaluated the effect of acute stress exposure on IL-6 gene expression levels

the 48-h time point. Cold exposure increased IL-6 expression in both chow-fed (p < 0.001, Figure 6J) and HFD-fed (p < 0.0001, Figure 6K) mice; however, the relative expression levels of IL-6 in HFD-fed cold-exposed mice were lower (p < 0.05, Figure 6L) when compared to those in chow-fed cold-exposed mice. Thus, cold exposure can partially restore the lPBN IL-6 loss in obesity.

lPBN as a Source of IL-6 for the PVH

Considering the impact of PBN IL-6 manipulation on body temperature and PVH-controlled HPT axis changes in the KD rats, the possibility of a direct neuronal link between the lPBN and PVH was further examined by a combination of retrograde tracer, AAV2(Retro)-eSyn-EGFP (Figure 7A), injected into the PVH (Figure 7B) and lPBN RNAscope (Figures 7E–7J). AAV-assisted retrograde neural tract tracing indicated the presence of retrogradedly labeled cell bodies specifically in the lPBN (Figure 7C), with an average of 18 cell bodies identified per each coronal section throughout the lPBN. Importantly, nearly all retrogardely labeled cell bodies contained IL-6 mRNA (Figures 7G–7J), indicating that lPBN neurons are one potential source of IL-6 in the PVH.

DISCUSSION

The cytokine IL-6 plays divergent roles in health and disease, supporting healthy weight maintenance in a normal physiological state, in addition to its role as an essential component of inflammatory response (Lutz, 2016; Rincon, 2012). Circulating levels of IL-6 are increased in obesity; however, these changes do not correspond with IL-6 levels in the CNS, which, instead, are reduced (Roytblat et al., 2000; Stenlöf et al., 2003). How and where the CNS production of IL-6 is affected by obesity remained poorly understood. Here, we show that obesity robustly affects brain IL-6 mRNA, and it does so in a neuroanatomically and sex-specific manner. Of the areas investigated, only lPBN was altered by IL-6. lPBN is a nucleus not as widely investigated as the hypothalamus, yet it is crucial in feeding control. Using recent advances in molecular and genetic tools, we were able to both localize IL-6 mRNA to neurons, astrocytes, and microglial cell bodies in lPBN and then selectively reduce IL-6 mRNA levels in the lPBN. This approach represents a significant refinement to many previous reports because localizing IL-6 to a specific brain region proved challenging because of a lack of reliable antibodies, and most manipulations of IL-6 involved whole body or, more recently, tissue/cell-specific manipulations, which are not compatible with understanding the diverse, and possibly divergent, function of IL-6 in different CNS nuclei (Erta et al., 2015; Matthews et al., 2010; Quintana et al., 2013; Wallenius et al., 2002b). Our complementary set of results clearly indicates that IL-6 acts in the lPBN to reduce the intake of chow and high-fat/high-sugar diet, and to increase BAT thermogenesis by increasing the HPT axis activity and sympathetic outflow. Moreover, IL-6 interacts with the adipose-produced hormone, leptin, at the level of the lPBN to reduce food intake, and its anorexic effect persists in high-fat/high-sugar diet-fed rats. Importantly, a reduction in lPBN IL-6 was detrimental to metabolic physiology, because it led to increased weight gain, increased adiposity, reduced BAT thermogenesis, and increased food intake.

Intra-lPBN delivery of exogenous IL-6 resulted in a significant hypophagia. Conversely, consistent with the anorexigenic role of IL-6 when delivered into the lPBN, the knockdown of IL-6 in this nucleus produced weight gain and long-term hyperphagia in rats fed a chow diet. The anorexic effect demonstrated here is in line with previous data indicating that IL-6 gene expression in the lPBN is increased by GLP-1R activation resulting in potent anorexia (Richard et al., 2014). Our results also suggest that the IL-6 produced in the lPBN likely acts locally within the lPBN, as IL-6 receptors are expressed locally and IL-6 mRNA is found in cells characterized by local peptide release: astrocytes, microglia, or (inter)neurons. Importantly, the lPBN IL-6 impact has the potential to extend beyond the lPBN, because we also found that IL-6-expressing lPBN neurons innervate the PVH. Moreover, in addition to the neuronal transport, lPBN-produced IL-6 may act at distant sites via CSF transport which has been demonstrated for other neuropeptides (Noble et al., 2018). Unlike the well-documented hypothalamic leptin resistance, the hypophagic effect of intra-lPBN delivered IL-6 persisted in obesity. However, it was not enhanced here, which was the case for intracerebroventricularly injected mice (Timper et al., 2017), potentially indicating that ventricular delivery of IL-6 may primarily act on brain nuclei other than the lPBN. Nonetheless, another study reports a blunted effect of IL-6 overexpression in obese mice, also at the level of the hypothalamus (Hidalgo et al., 2010). Thus, the action of endogenously versus exogenously produced ligand may be the determining factor in detection of a blunted effect in obesity. This idea is also consistent with the otherwise surprising finding, that the increased weight gain and food intake of lPBN IL-6 KD rats disappeared in high-fat/high-sugar diet-fed rats. However, these results are consistent with reports on the whole-body IL-6 knockout HFD-fed mice from the Febbraio laboratory (Matthews et al., 2010). Thus, this phenomenon persists across species and diets. At this point, we can only speculate on the mechanism, but the most fitting hypothesis would be that because obesity reduces CSF and lPBN IL-6 levels, this reduction masks the relatively smaller effect of the knockdown, reducing the possibility for detection of any further phenotype changes.

We show that leptin, at the level of the lPBN, reduces food intake, in line with previous data (Alhadeff et al., 2014b), and, in contrast to IL-6, it does not affect thermoregulation. Because leptin receptors share certain downstream signaling with IL-6Rα, for example, STAT3 (Dunn-Meynell et al., 2016), leptin and IL-6 both can be classified as cytokines and are related structurally, and both ligands produce anorexia by acting on the lPBN, we hypothesized a synergistic relationship between leptin and IL-6 in this area. In line with our hypothesis, injection of subthreshold doses of both ligands produced a clear reduction in feeding when co-applied to the lPBN indicating that IL-6 can amplify leptin's anorexic effects at the level of the lPBN.

The lPBN is neuroanatomically perfectly positioned to regulate food intake but it also plays a critical role in thermogenesis. A wealth of data suggests that it receives sensory information on internal, as well as skin temperature (Geerling et al., 2016; Kobayashi and Osaka, 2003; Sato et al., 2015; Yahiro et al.,
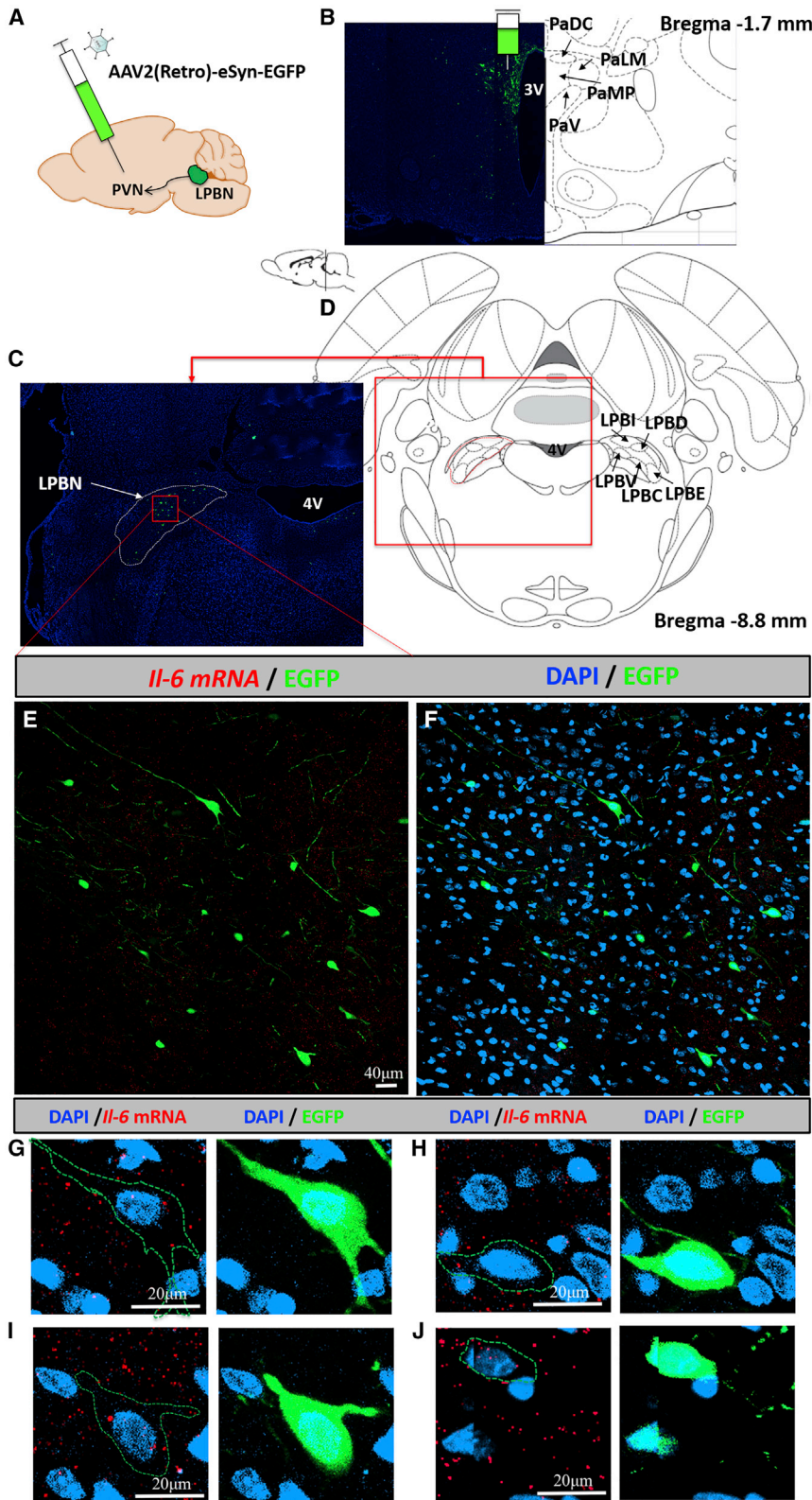
Figure 7. Lateral PBN IL-6-Expressing Neurons Innervate the Paraventricular Hypothalamus

(A) Retrograde viral tracer was unilaterally injected into the paraventricular hypothalamus of two 6-week-old male rats at a volume of 0.5 μL. Tissues were harvested 3 weeks later.

(B) Representative confocal image of the retrograde viral tracer injection site along with the corresponding rat brain atlas slide to show the confinement of the viral infection to the paraventricular hypothalamus.

(C and D) The densest PBN area of green fluorescent protein (EGFP)-labeled neurons was located in the lPBN (C) and the corresponding rat brain atlas slide (D).

(E and F) Lateral PBN-focused images show cell bodies labeled with EGFP retrogradely carried from the paraventricular hypothalamus without (E) and with (F) DAPI. Interleukin-6 mRNA expression, detected by RNAscope *in situ* hybridization and shown in red, throughout the same area of lPBN.

(G–J) Four examples of high-resolution cell images to show IL-6 mRNA (red) in the lPBN neurons projecting to the PVH (green). The green serrated line represents a trace of the green EGFP label (to outline the cell body and fibers in the image) and is superimposed on the RNAscope image in order to reveal the signal in the cell that is otherwise made less visible by the strong EGFP label. Cell nuclei are labeled in blue with DAPI. 4V, fourth ventricle; PVN, paraventricular nucleus; PaDC, paraventricular hypothalamic nucleus, dorsal cap; PaV, paraventricular hypothalamic nucleus, ventral part; PaMP, paraventricular hypothalamic nucleus, medial parvicellular part; PaLM, paraventricular hypothalamic nucleus, lateral magnocellular part; LPBI, lateral parabrachial nucleus, internal part; LPBD, lateral parabrachial nucleus, dorsal part; LPBV, lateral parabrachial nucleus, ventral part; LPBC, lateral parabrachial nucleus, central part; LPBE, lateral parabrachial nucleus, external part.

2017), and sends outputs to the forebrain and the hindbrain thermoregulatory hubs, including the PVH and *raphe pallidus* (RPa). It is involved in the central mechanisms of cooling-induced thermogenesis, and loss of PBN leads to inadequate thermogenic adaptation in cool ambient temperatures (Geerling et al., 2016; Kobayashi and Osaka, 2003; Yahiro et al., 2017). Our data place IL-6 as an essential component of PBN thermoregulatory function. Acute exogenous delivery of IL-6 to the lPBN led to fast onset hyperthermia, likely driven by increased BAT thermogenesis. Conversely, reduction of IL-6 production in the lPBN by anti-IL-6 siRNA led to a persistent reduction in core and BAT temperatures. Importantly, the observed changes in thermogenesis are unlikely to be driven by alterations in motor activity, as neither exogenous IL-6 nor knockdown of IL-6 gene expression altered home-cage locomotor activity, measured and analyzed every minute for 2 days and 2 nights. Yet, significant changes in body temperature were recorded during the same time period.

The molecular profile of BAT also supported reduced thermogenic capacity after lPBN IL-6 loss, as *ucp-1, dio2*, and *prdm16* gene expression was potently suppressed. This idea is further supported by reduction in UCP-1 protein in BAT. Alterations in sympathetic nervous system output or the thyroid axis are two critical mechanisms of CNS thermoregulatory control; both were affected by IL-6 lPBN loss, indicating the robust multipronged capacity of IL-6 to alter thermogenic output. The thermogenic capacity of BAT is orchestrated by the CNS and relies on the activity of the sympathetic nervous system (Burgi et al., 2011; Cannon and Nedergaard, 2004; Contreras et al., 2015). The thyroid system can act at the central level and stimulate the sympathetic tone to increase the thermogenic activity of BAT (López et al., 2013). Based on the direct neuroanatomical outputs of the lPBN it is plausible that thyroid axis and sympathetic output are directly affected by lPBN neurons projecting to the PVH or RPa (Saper and Loewy, 1980). This is supported by our data showing lPBN neuronal fibers in the PVH (a route for potential neuronal transport of IL-6 from PBN to PVH) and IL-6 receptor expression in the PVH (Schéle et al., 2012). Considering the diet-induced obesity-associated reduction of IL-6 in the entire lPBN shown here, it is likely that PVH-projecting neurons specifically also display reduced IL-6 in obesity, although future studies should evaluate this question directly. Thus, reduced lPBN IL-6 has the potential to affect the lPBN-PVH link; disruption in this communication may be one of the mechanisms via which IL-6 reduction disrupts thermogenesis and exacerbates weight gain. However, as there are relatively few PVH-projecting neurons, it is unlikely to be the only mechanism disrupted by lPBN IL-6 gene expression reduction. In addition to lPBN-PVH link route, it is also possible that the reduced plasma T3 levels are a consequence of reduced SNS output to BAT, and following reduction of DIO2 (Castillo et al., 2011; Christoffolete et al., 2004; Fonseca et al., 2014), both detected here. The latter idea is also consistent with the increased TRH gene expression in the PVH.

Exposure of animals to cold environments potently triggers thermo-effectors, including BAT thermogenesis, to maintain body temperature. Here, we show that 48 h exposure to 4°C potently (4- to 8-fold) upregulated IL-6 gene expression in mice, consistent with its thermogenic role demonstrated here. Moreover, this upregulation persisted in the HFD-fed mice.

This is important, because it indicates that the IL-6 deficit in the PBN of obese mice is diet/obesity-specific and can be bypassed by other inputs like cold exposure. Thus, cold exposure can be utilized to "normalize" (though not completely) the obesity-suppressed IL-6 levels.

However, the PBN IL-6 is still selective in its sensitivity to thermogenic factors, because acute stress, shown to reliably induce a psychogenic fever, by, for example, engaging the preoptic hypothalamus temperature sensitive neurons (Kataoka et al., 2014), did not affect lPBN IL-6 gene expression. This lack of effect under stress is also consistent with the lack of consistent changes in the anxiety-like phenotype in lPBN IL-6 KD rats or unaffected *Crh* gene expression in the PVH of these rats. Reduction in lPBN IL-6 was associated with reduced time spent in the center of the open field test, with no significant effect in another test of anxiety, the EPM test. However, in both tests, we find a reduced locomotor activity. Collectively these data led us to conclude that it is more likely that these animals have either a reduced tendency for novelty-induced activity and/or a higher sensitivity for stress-induced locomotor suppression, suggesting that some aspects of emotional reactivity are affected. Notably, chronic unpredictable stress is associated with elevated IL-6 in other brain regions, for example, the hippocampus (Tianzhu et al., 2014), again potentially indicating divergence of function dictated by the neuroanatomical location. Additionally, chronic stress was previously shown to increase BBB permeability to peripheral circulating IL-6 (via alteration in tight junction protein) in nucleus accumbens, and, thus, it is possible that increased protein levels in other brain tissues after stress reflect this process (Menard et al., 2017). Although, also the difference in chronic versus acute stress cannot be discounted when comparing the two datasets.

PBN is an important node mediating infection-associated anorexia, and IL-6 is one of the signaling steps needed for anorexia of infection to take place (Langhans and Geary, 2010). Although our current data clearly show that IL-6 in the PBN is a critical element for body weight and intake homeostasis during health, we cannot eliminate the possibility that this pathway gets hijacked during disease or by disease-mimicking agents (e.g., lipopolysaccharide treatment) to promote anorexia during infection.

Several factors may have contributed to the lack of reduction in PBN IL-6 in obese females, or lack of increase in PBN IL-6 in cold-exposed females, in contrast to males. In fact, the relationship of sex, estrogens, and IL-6 is equally complex as that of IL-6 and obesity, with estrogens reducing IL-6 in various pathological contexts during infection or liver cancer (Liu et al., 2014; Naugler et al., 2007). However, estradiol replacement therapy does not alter IL-6 levels in postmenopausal women (Edwards and Mills, 2008), and, higher, lower, or similar levels of IL-6 have been measured in healthy men versus women (Giraldo et al., 2008). Sex differences in the role of CNS produced IL-6 have already been indicated (Erta et al., 2015). We have previously demonstrated that estrous females have higher GLP-1R-induced IL-6 mRNA levels in the hypothalamus when circulating estrogen levels are highest (López-Ferreras et al., 2018). Thus, is possible that higher estrogen levels in females compared to males protect from obesity-driven IL-6 reduction. It is also possible that in

females the diet simply takes longer to affect PBN IL-6; females are able to better defend themselves against the reduction. Sex differences in brain IL-6 production is certainly a topic that deserves the focused attention of a future study.

In conclusion (graphical abstract), we demonstrate that IL-6 can be produced by lPBN neurons, astrocytes, and microglia. It acts at the level of the lPBN to reduce body weight by increasing BAT thermogenesis and by reducing food intake, but it can also reach CNS areas outside of the PBN (e.g., PVH). We identify two (patho)physiological contexts, obesity and cold exposure, which divergently affect IL-6 production specifically in the lPBN. We also show that the obesity-induced IL-6 deficit can be bypassed by cold exposure and that the deficit is not present for exogenous IL-6 application. The latter point, along with the identified here cooperative interaction of exogenously applied IL-6 with leptin in the lPBN, highlights the emerging potential importance of the local circuit identified here for development of obesity therapeutics.

STAR★METHODS

Detailed methods are provided in the online version of this paper and include the following:

- KEY RESOURCES TABLE
- CONTACT FOR REAGENT AND RESOURCE SHARING
- EXPERIMENTAL MODEL AND SUBJECT DETAILS
- METHOD DETAILS
  - Quantitative PCR
  - Drugs
  - Intracranial cannulation and injections
  - lPBN IL-6 gene knockdown
  - Acute food intake measurements
  - Telemetric measurements
  - Brown adipose tissue (BAT) temperature measurements
  - Anxiety-like behavior evaluation
  - Acute Stress
  - Blood biochemistry
  - Brown adipose tissue immunohistochemistry
  - *In situ* hybridization using RNAScope
  - RNAScope for fixed frozen sections
  - Acute cold exposure
  - Protein extraction and western blot
  - Neural tract tracing: Brain tissue preparation and imaging
- QUANTIFICATION AND STATISTICAL ANALYSIS

SUPPLEMENTAL INFORMATION

Supplemental Information includes seven figures and can be found with this article online at https://doi.org/10.1016/j.celrep.2019.02.044.

REFERENCES

Alhadeff, A.L., Baird, J.P., Swick, J.C., Hayes, M.R., and Grill, H.J. (2014a). Glucagon-like Peptide-1 receptor signaling in the lateral parabrachial nucleus contributes to the control of food intake and motivation to feed. Neuropsychopharmacology *39*, 2233–2243.

Alhadeff, A.L., Hayes, M.R., and Grill, H.J. (2014b). Leptin receptor signaling in the lateral parabrachial nucleus contributes to the control of food intake. Am. J. Physiol. Regul. Integr. Comp. Physiol. *307*, R1338–R1344.

Anesten, F., Santos, C., Gidestrand, E., Schéle, E., Pálsdóttir, V., Swedung-Wettervik, T., Meister, B., Patrycja Skibicka, K., and Jansson, J.O. (2017). Functional interleukin-6 receptor-α is located in tanycytes at the base of the third ventricle. J. Neuroendocrinol. *29*. https://doi.org/10.1111/jne.12546.

Bastard, J.P., Jardel, C., Bruckert, E., Blondy, P., Capeau, J., Laville, M., Vidal, H., and Hainque, B. (2000). Elevated levels of interleukin 6 are reduced in serum and subcutaneous adipose tissue of obese women after weight loss. J. Clin. Endocrinol. Metab. *85*, 3338–3342.

Benrick, A., Schéle, E., Pinnock, S.B., Wernstedt-Asterholm, I., Dickson, S.L., Karlsson-Lindahl, L., and Jansson, J.O. (2009). Interleukin-6 gene knockout influences energy balance regulating peptides in the hypothalamic paraventricular and supraoptic nuclei. J. Neuroendocrinol. *21*, 620–628.

Bernard, J.F., Bester, H., and Besson, J.M. (1996). Involvement of the spino-parabrachio -amygdaloid and -hypothalamic pathways in the autonomic and affective emotional aspects of pain. Prog. Brain Res. *107*, 243–255.

Bianco, A.C., and Silva, J.E. (1987a). Intracellular conversion of thyroxine to triiodothyronine is required for the optimal thermogenic function of brown adipose tissue. J. Clin. Invest. *79*, 295–300.

Bianco, A.C., and Silva, J.E. (1987b). Nuclear 3,5,3′-triiodothyronine (T3) in brown adipose tissue: receptor occupancy and sources of T3 as determined by in vivo techniques. Endocrinology *120*, 55–62.

Bodnar, R.J. (2018). Conditioned flavor preferences in animals: merging pharmacology, brain sites and genetic variance. Appetite *122*, 17–25.

Burgi, K., Cavalleri, M.T., Alves, A.S., Britto, L.R.G., Antunes, V.R., and Michelini, L.C. (2011). Tyrosine hydroxylase immunoreactivity as indicator of sympathetic activity: simultaneous evaluation in different tissues of hypertensive rats. Am. J. Physiol. Regul. Integr. Comp. Physiol. *300*, R264–R271.

Cannon, B., and Nedergaard, J. (2004). Brown adipose tissue: function and physiological significance. Physiol. Rev. *84*, 277–359.

Castillo, M., Hall, J.A., Correa-Medina, M., Ueta, C., Kang, H.W., Cohen, D.E., and Bianco, A.C. (2011). Disruption of thyroid hormone activation in type 2 deiodinase knockout mice causes obesity with glucose intolerance and liver steatosis only at thermoneutrality. Diabetes 60, 1082–1089.

Chida, D., Osaka, T., Hashimoto, O., and Iwakura, Y. (2006). Combined interleukin-6 and interleukin-1 deficiency causes obesity in young mice. Diabetes 55, 971–977.

Christoffolete, M.A., Linardi, C.C., de Jesus, L., Ebina, K.N., Carvalho, S.D., Ribeiro, M.O., Rabelo, R., Curcio, C., Martins, L., Kimura, E.T., and Bianco, A.C. (2004). Mice with targeted disruption of the Dio2 gene have cold-induced overexpression of the uncoupling protein 1 gene but fail to increase brown adipose tissue lipogenesis and adaptive thermogenesis. Diabetes 53, 577–584.

Contreras, C., Gonzalez, F., Fernø, J., Diéguez, C., Rahmouni, K., Nogueiras, R., and López, M. (2015). The brain and brown fat. Ann. Med. 47, 150–168.

Della Vedova, M.C., Muñoz, M.D., Santillan, L.D., Plateo-Pignatari, M.G., Germanó, M.J., Rinaldi Tosi, M.E., Garcia, S., Gomez, N.N., Fornes, M.W., Gomez Mejiba, S.E., and Ramirez, D.C. (2016). A mouse model of diet-induced obesity resembling most features of human metabolic syndrome. Nutr. Metab. Insights 9, 93–102.

Diepenbroek, C., Eggels, L., Ackermans, M.T., Fliers, E., Kalsbeek, A., Serlie, M.J., and la Fleur, S.E. (2017). Differential effects of hypercaloric choice diets on insulin sensitivity in rats. J. Endocrinol. 232, 49–57.

Dunn-Meynell, A.A., Le Foll, C., Johnson, M.D., Lutz, T.A., Hayes, M.R., and Levin, B.E. (2016). Endogenous VMH amylin signaling is required for full leptin signaling and protection from diet-induced obesity. Am. J. Physiol. Regul. Integr. Comp. Physiol. 310, R355–R365.

Edwards, K.M., and Mills, P.J. (2008). Effects of estrogen versus estrogen and progesterone on cortisol and interleukin-6. Maturitas 61, 330–333.

Elmquist, J.K., Bjørbaek, C., Ahima, R.S., Flier, J.S., and Saper, C.B. (1998). Distributions of leptin receptor mRNA isoforms in the rat brain. J. Comp. Neurol. 395, 535–547.

Erta, M., Quintana, A., and Hidalgo, J. (2012). Interleukin-6, a major cytokine in the central nervous system. Int. J. Biol. Sci. 8, 1254–1266.

Erta, M., Giralt, M., Esposito, F.L., Fernandez-Gayol, O., and Hidalgo, J. (2015). Astrocytic IL-6 mediates locomotor activity, exploration, anxiety, learning and social behavior. Horm. Behav. 73, 64–74.

Febbraio, M.A., Rose-John, S., and Pedersen, B.K. (2010). Is interleukin-6 receptor blockade the Holy Grail for inflammatory diseases? Clin. Pharmacol. Ther. 87, 396–398.

Flak, J.N., Patterson, C.M., Garfield, A.S., D'Agostino, G., Goforth, P.B., Sutton, A.K., Malec, P.A., Wong, J.T., Germani, M., Jones, J.C., et al. (2014). Leptin-inhibited PBN neurons enhance responses to hypoglycemia in negative energy balance. Nat. Neurosci. 17, 1744–1750.

Fonseca, T.L., Werneck-De-Castro, J.P., Castillo, M., Bocco, B.M., Fernandes, G.W., McAninch, E.A., Ignacio, D.L., Moises, C.C., Ferreira, A.R., Gereben, B., and Bianco, A.C. (2014). Tissue-specific inactivation of type 2 deiodinase reveals multilevel control of fatty acid oxidation by thyroid hormone in the mouse. Diabetes 63, 1594–1604.

Gallistl, S., Sudi, K.M., Aigner, R., and Borkenstein, M. (2001). Changes in serum interleukin-6 concentrations in obese children and adolescents during a weight reduction program. Int. J. Obes. Relat. Metab. Disord. 25, 1640–1643.

Gauriau, C., and Bernard, J.F. (2002). Pain pathways and parabrachial circuits in the rat. Exp. Physiol. 87, 251–258.

Geerling, J.C., Kim, M., Mahoney, C.E., Abbott, S.B., Agostinelli, L.J., Garfield, A.S., Krashes, M.J., Lowell, B.B., and Scammell, T.E. (2016). Genetic identity of thermosensory relay neurons in the lateral parabrachial nucleus. Am. J. Physiol. Regul. Integr. Comp. Physiol. 310, R41–R54.

Giraldo, E., Hinchado, M.D., Garcia, J.J., and Ortega, E. (2008). Influence of gender and oral contraceptives intake on innate and inflammatory response. Role of neuroendocrine factors. Mol. Cell. Biochem. 313, 147–153.

Grill, H.J., Schwartz, M.W., Kaplan, J.M., Foxhall, J.S., Breininger, J., and Baskin, D.G. (2002). Evidence that the caudal brainstem is a target for the inhibitory effect of leptin on food intake. Endocrinology 143, 239–246.

Harms, M.J., Ishibashi, J., Wang, W., Lim, H.W., Goyama, S., Sato, T., Kurokawa, M., Won, K.J., and Seale, P. (2014). Prdm16 is required for the maintenance of brown adipocyte identity and function in adult mice. Cell Metab. 19, 593–604.

Hidalgo, J., Florit, S., Giralt, M., Ferrer, B., Keller, C., and Pilegaard, H. (2010). Transgenic mice with astrocyte-targeted production of interleukin-6 are resistant to high-fat diet-induced increases in body weight and body fat. Brain Behav. Immun. 24, 119–126.

Hodes, G.E., Ménard, C., and Russo, S.J. (2016). Integrating Interleukin-6 into depression diagnosis and treatment. Neurobiol. Stress 4, 15–22.

Hosoi, T., Okuma, Y., and Nomura, Y. (2002). Leptin regulates interleukin-1beta expression in the brain via the STAT3-independent mechanisms. Brain Res. 949, 139–146.

Kataoka, N., Hioki, H., Kaneko, T., and Nakamura, K. (2014). Psychological stress activates a dorsomedial hypothalamus-medullary raphe circuit driving brown adipose tissue thermogenesis and hyperthermia. Cell Metab. 20, 346–358.

Kobayashi, A., and Osaka, T. (2003). Involvement of the parabrachial nucleus in thermogenesis induced by environmental cooling in the rat. Pflugers Arch. 446, 760–765.

Langhans, W., and Geary, N. (2010). Overview of the physiological control of eating. Forum Nutr. 63, 9–53.

Larsen, L., Le Foll, C., Dunn-Meynell, A.A., and Levin, B.E. (2016). IL-6 ameliorates defective leptin sensitivity in DIO ventromedial hypothalamic nucleus neurons. Am. J. Physiol. Regul. Integr. Comp. Physiol. 311, R764–R770.

Le Foll, C., Johnson, M.D., Dunn-Meynell, A.A., Boyle, C.N., Lutz, T.A., and Levin, B.E. (2015). Amylin-induced central IL-6 production enhances ventromedial hypothalamic leptin signaling. Diabetes 64, 1621–1631.

Lee, S.J., Sanchez-Watts, G., Krieger, J.P., Pignalosa, A., Norell, P.N., Cortella, A., Pettersen, K.G., Vrdoljak, D., Hayes, M.R., Kanoski, S.E., et al. (2018). Loss of dorsomedial hypothalamic GLP-1 signaling reduces BAT thermogenesis and increases adiposity. Mol. Metab. 11, 33–46.

Lin, S., Thomas, T.C., Storlien, L.H., and Huang, X.F. (2000). Development of high fat diet-induced obesity and leptin resistance in C57Bl/6J mice. Int. J. Obes. Relat. Metab. Disord. 24, 639–646.

Liu, L., Zhao, Y., Xie, K., Sun, X., Jiang, L., Gao, Y., and Wang, Z. (2014). Estrogen inhibits LPS-induced IL-6 production in macrophages partially via the nongenomic pathway. Immunol. Invest. 43, 693–704.

Livak, K.J., and Schmittgen, T.D. (2001). Analysis of relative gene expression data using real-time quantitative PCR and the 2(-Delta Delta C(T)) Method. Methods 25, 402–408.

López, M., Varela, L., Vázquez, M.J., Rodríguez-Cuenca, S., González, C.R., Velagapudi, V.R., Morgan, D.A., Schoenmakers, E., Agassandian, K., Lage, R., et al. (2010). Hypothalamic AMPK and fatty acid metabolism mediate thyroid regulation of energy balance. Nat. Med. 16, 1001–1008.

López, M., Alvarez, C.V., Nogueiras, R., and Diéguez, C. (2013). Energy balance regulation by thyroid hormones at central level. Trends Mol. Med. 19, 418–427.

López-Ferreras, L., Richard, J.E., Noble, E.E., Eerola, K., Anderberg, R.H., Olandersson, K., Taing, L., Kanoski, S.E., Hayes, M.R., and Skibicka, K.P. (2018). Lateral hypothalamic GLP-1 receptors are critical for the control of food reinforcement, ingestive behavior and body weight. Mol. Psychiatry 23, 1157–1168.

Lutz, T.A. (2016). The brain needs interleukin-6 (IL-6) to maintain a "healthy" energy balance. Focus on "IL-6 ameliorates defective leptin sensitivity in DIO ventromedial hypothalamic nucleus neurons". Am. J. Physiol. Regul. Integr. Comp. Physiol. 311, R989–R991.

Maniscalco, J.W., Zheng, H., Gordon, P.J., and Rinaman, L. (2015). Negative energy balance blocks neural and behavioral responses to acute stress

by "silencing" central glucagon-like peptide 1 signaling in rats. J. Neurosci. *35*, 10701–10714.

Martinez-Sanchez, N., Seoane-Collazo, P., Contreras, C., Varela, L., Villarroya, J., Rial-Pensado, E., Buque, X., Aurrekoetxea, I., Delgado, T.C., Vazquez-Martinez, R., et al. (2017). Hypothalamic AMPK-ER Stress-JNK1 axis mediates the central actions of thyroid hormones on energy balance. Cell Metab. *26*, 212–229.e12.

Matesanz, N., Bernardo, E., Acín-Pérez, R., Manieri, E., Pérez-Sieira, S., Hernández-Cosido, L., Montalvo-Romeral, V., Mora, A., Rodríguez, E., Leiva-Vega, L., et al. (2017). MKK6 controls T3-mediated browning of white adipose tissue. Nat. Commun. *8*, 856.

Matthews, V.B., Allen, T.L., Risis, S., Chan, M.H., Henstridge, D.C., Watson, N., Zaffino, L.A., Babb, J.R., Boon, J., Meikle, P.J., et al. (2010). Interleukin-6-deficient mice develop hepatic inflammation and systemic insulin resistance. Diabetologia *53*, 2431–2441.

Menard, C., Pfau, M.L., Hodes, G.E., Kana, V., Wang, V.X., Bouchard, S., Takahashi, A., Flanigan, M.E., Aleyasin, H., LeClair, K.B., et al. (2017). Social stress induces neurovascular pathology promoting depression. Nat. Neurosci. *20*, 1752–1760.

Myers, K.P. (2018). The convergence of psychology and neurobiology in flavor-nutrient learning. Appetite *122*, 36–43.

Naugler, W.E., Sakurai, T., Kim, S., Maeda, S., Kim, K., Elsharkawy, A.M., and Karin, M. (2007). Gender disparity in liver cancer due to sex differences in MyD88-dependent IL-6 production. Science *317*, 121–124.

Noble, E.E., Hahn, J.D., Konanur, V.R., Hsu, T.M., Page, S.J., Cortella, A.M., Liu, C.M., Song, M.Y., Suarez, A.N., Szujewski, C.C., et al. (2018). Control of feeding behavior by cerebral ventricular volume transmission of melanin-concentrating hormone. Cell Metab. *28*, 55–68.e7.

Obregon, M.J. (2014). Adipose tissues and thyroid hormones. Front. Physiol. *5*, 479.

Quintana, A., Erta, M., Ferrer, B., Comes, G., Giralt, M., and Hidalgo, J. (2013). Astrocyte-specific deficiency of interleukin-6 and its receptor reveal specific roles in survival, body weight and behavior. Brain Behav. Immun. *27*, 162–173.

Richard, J.E., Farkas, I., Anesten, F., Anderberg, R.H., Dickson, S.L., Gribble, F.M., Reimann, F., Jansson, J.O., Liposits, Z., and Skibicka, K.P. (2014). GLP-1 receptor stimulation of the lateral parabrachial nucleus reduces food intake: neuroanatomical, electrophysiological, and behavioral evidence. Endocrinology *155*, 4356–4367.

Rincon, M. (2012). Interleukin-6: from an inflammatory marker to a target for inflammatory diseases. Trends Immunol. *33*, 571–577.

Roytblat, L., Rachinsky, M., Fisher, A., Greemberg, L., Shapira, Y., Douvdevani, A., and Gelman, S. (2000). Raised interleukin-6 levels in obese patients. Obes. Res. *8*, 673–675.

Saper, C.B., and Loewy, A.D. (1980). Efferent connections of the parabrachial nucleus in the rat. Brain Res. *197*, 291–317.

Sato, M., Ito, M., Nagase, M., Sugimura, Y.K., Takahashi, Y., Watabe, A.M., and Kato, F. (2015). The lateral parabrachial nucleus is actively involved in the acquisition of fear memory in mice. Mol. Brain *8*, 22.

Schéle, E., Fekete, C., Egri, P., Füzesi, T., Palkovits, M., Keller, É., Liposits, Z., Gereben, B., Karlsson-Lindahl, L., Shao, R., and Jansson, J.O. (2012). Interleukin-6 receptor α is co-localised with melanin-concentrating hormone in human and mouse hypothalamus. J. Neuroendocrinol. *24*, 930–943.

Sclafani, A. (2016). Bypassing intestinal sugar enhancement of sweet appetite. Cell Metab. *23*, 3–4.

Sclafani, A., and Ackroff, K. (2016). Operant licking for intragastric sugar infusions: Differential reinforcing actions of glucose, sucrose and fructose in mice. Physiol. Behav. *153*, 115–124.

Shah, B.P., Vong, L., Olson, D.P., Koda, S., Krashes, M.J., Ye, C., Yang, Z., Fuller, P.M., Elmquist, J.K., and Lowell, B.B. (2014). MC4R-expressing glutamatergic neurons in the paraventricular hypothalamus regulate feeding and are synaptically connected to the parabrachial nucleus. Proc. Natl. Acad. Sci. USA *111*, 13193–13198.

Shirazi, R., Palsdottir, V., Collander, J., Anesten, F., Vogel, H., Langlet, F., Jaschke, A., Schürmann, A., Prévot, V., Shao, R., et al. (2013). Glucagon-like peptide 1 receptor induced suppression of food intake, and body weight is mediated by central IL-1 and IL-6. Proc. Natl. Acad. Sci. USA *110*, 16199–16204.

Skibicka, K.P., and Grill, H.J. (2009). Hindbrain leptin stimulation induces anorexia and hyperthermia mediated by hindbrain melanocortin receptors. Endocrinology *150*, 1705–1711.

Stenlöf, K., Wernstedt, I., Fjällman, T., Wallenius, V., Wallenius, K., and Jansson, J.O. (2003). Interleukin-6 levels in the central nervous system are negatively correlated with fat mass in overweight/obese subjects. J. Clin. Endocrinol. Metab. *88*, 4379–4383.

Tianzhu, Z., Shihai, Y., and Juan, D. (2014). Antidepressant-like effects of cordycepin in a mice model of chronic unpredictable mild stress. Evid. Based Complement. Alternat. Med. *2014*, 438506.

Timper, K., Denson, J.L., Steculorum, S.M., Heilinger, C., Engström-Ruud, L., Wunderlich, C.M., Rose-John, S., Wunderlich, F.T., and Brüning, J.C. (2017). IL-6 improves energy and glucose homeostasis in obesity via enhanced central IL-6 trans-signaling. Cell Rep. *19*, 267–280.

Ulrich-Lai, Y.M., Christiansen, A.M., Ostrander, M.M., Jones, A.A., Jones, K.R., Choi, D.C., Krause, E.G., Evanson, N.K., Furay, A.R., Davis, J.F., et al. (2010). Pleasurable behaviors reduce stress via brain reward pathways. Proc. Natl. Acad. Sci. USA *107*, 20529–20534.

Ulrich-Lai, Y.M., Ostrander, M.M., and Herman, J.P. (2011). HPA axis dampening by limited sucrose intake: reward frequency vs. caloric consumption. Physiol. Behav. *103*, 104–110.

Ulrich-Lai, Y.M., Fulton, S., Wilson, M., Petrovich, G., and Rinaman, L. (2015). Stress exposure, food intake and emotional state. Stress *18*, 381–399.

Varela, L., Martínez-Sánchez, N., Gallego, R., Vázquez, M.J., Roa, J., Gándara, M., Schoenmakers, E., Nogueiras, R., Chatterjee, K., Tena-Sempere, M., et al. (2012). Hypothalamic mTOR pathway mediates thyroid hormone-induced hyperphagia in hyperthyroidism. J. Pathol. *227*, 209–222.

Wallenius, K., Wallenius, V., Sunter, D., Dickson, S.L., and Jansson, J.O. (2002a). Intracerebroventricular interleukin-6 treatment decreases body fat in rats. Biochem. Biophys. Res. Commun. *293*, 560–565.

Wallenius, V., Wallenius, K., Ahrén, B., Rudling, M., Carlsten, H., Dickson, S.L., Ohlsson, C., and Jansson, J.O. (2002b). Interleukin-6-deficient mice develop mature-onset obesity. Nat. Med. *8*, 75–79.

Wu, Q., Boyle, M.P., and Palmiter, R.D. (2009). Loss of GABAergic signaling by AgRP neurons to the parabrachial nucleus leads to starvation. Cell *137*, 1225–1234.

Yahiro, T., Kataoka, N., Nakamura, Y., and Nakamura, K. (2017). The lateral parabrachial nucleus, but not the thalamus, mediates thermosensory pathways for behavioural thermoregulation. Sci. Rep. *7*, 5031.

STAR★METHODS

KEY RESOURCES TABLE

REAGENT or RESOURCE	SOURCE	IDENTIFIER
Critical Commercial Assays		
IL-6	Applied Biosystems	Assay ID Mm00446190_m1
IL-6-Ra	Applied Biosystems	Assay ID Mm00439653_m1
IL-1b	Applied Biosystems	Assay ID Mm00434228_m1
TNFa	Applied Biosystems	Assay ID Mm00443258_m1
IL-6 (rat)	Applied Biosystems	Assay ID Rn01410330_m1
Dio2	Applied Biosystems	Assay ID Rn00581867_m1
Prdm16	Applied Biosystems	Assay ID Rn01516224_m1
UCP1	Applied Biosystems	Assay ID Rn00562126_m1
Trh	Applied Biosystems	Assay ID Rn00564880_m1
Tshb	Applied Biosystems	Assay ID Rn00565424_m1
Crh	Applied Biosystems	Assay ID Rn01462137_m1
IL-6 (RNAscope)	Advanced Cell Diagnostics	Probe ID Rn-IL-6-C3; cat# 427141 C3
GFAP (RNAscope)	Advanced Cell Diagnostics	Probe ID Rn-GFAP-C1; cat# 407881
Rbfox3 (RNAscope)	Advanced Cell Diagnostics	Probe ID Rn-Rbfox3-C1; cat# 436351
AIF1 (RNAscope)	Advanced Cell Diagnostics	Probe ID Rn-Aif1-C2; cat# 457731-C2
3-Plex negative control	Advanced Cell Diagnostics	Cat# 320871
Bacterial and Virus Strains		
IL-6 AAV siRNA pooled virus, Serotype 2	ABM	Cat# iAAV01087702
Scrambled AAV siRNA control virus, Serotype 2	ABM	Cat# iiAAV01502
AAV2(Retro)-eSyn-EGFP	Vector Biolabs	N/A, custom made
Experimental Models: Organisms/Strains		
Sprague-Dawley rats	Charles River	Strain ID: CD
C57BL/6 mice	Charles River	Strain of origin: C57BL/6N
Chemicals, Peptides, and Recombinant Proteins		
Interleukin-6 (IL-6)	Peprotech	Cat# 400-05
Rat Recombinant Leptin	Peprotech	Cat# 400-21
Software and Algorithms		
VitalView 5.0	Koninklijke Philips Electronics N.V.	N/A
Prism 7	GraphPad Software	https://www.graphpad.com/
IMAGEJ	NIH	https://imagej.nih.gov/ij/
MED-SYST-8A	Med Associates	N/A
Zen Lite	Zeiss	https://www.zeiss.com/microscopy/int/products/microscope-software/zen-lite.html
Other		
High-fat diet for mice (HFD)	Research Diets	Cat# D12492
Normal chow diet	Harlan-Teklad	Global Diet Cat# 2016
E-mitter for temperature and activity measurements	Minimitter	Probe ID G2
E-mitter for heart rate, temperature, and activity	Minimitter	Probe ID HRC 4000
Infrared camera	FLIR	Model# T-500

CONTACT FOR REAGENT AND RESOURCE SHARING

Further information and requests for resources and reagents should be directed to and will be fulfilled by the Lead Contact, Karolina P. Skibicka (Karolina.Skibicka@neuro.gu.se).

EXPERIMENTAL MODEL AND SUBJECT DETAILS

Five-week-old male and female C57BL/6N mice were fed regular chow (Global Diet #2016; Harlan-Teklad; 4% kcal from fat) or HFD (catalog #D12492; Research Diets Inc.; 60% kcal from fat) over 8 weeks. Male or female Sprague-Dawley CD rats (5 weeks at arrival, Charles River, Germany) were individually housed in cages with *ad libitum* access to either chow and water; or exposed to high-fat/high-sugar diet consisting of *ad libitum* access to chow, in-house made 50/50% by weight sucrose/lard mixture, and water. Additional experiments (Figures 2 and S6) were conducted in rats fed chow, or obesogenic diet consisting of *ad libitum* access to chow, lard, sucrose solution (30% sucrose), and water to allow for recording of intake of fat and sugar separately after treatments. All rodents were maintained on a 12h/12h light/dark cycle. All studies were approved by the Animal Welfare Committee of the University of Pennsylvania or University of Gothenburg, Sweden, Ethical permit # 137/15, 195/13, and 77/15.

METHOD DETAILS

Quantitative PCR

All rat or mouse brains were rapidly extracted after light (4%) isoflurane (Baxter AB, Sweden) anesthesia, quickly frozen in isopentane (on dry ice chamber) and transferred to $-80°C$ freezer; PBN, hypothalamus, amygdala, and hippocampus were collected. Note that while for rat brain dissections lPBN was reliably dissected, in mice the dissections likely encompassed lateral and dorsal parts of the mPBN. Total RNA was extracted using RNeasy Lipid Tissue Mini kit (QIAGEN) with additional deoxy ribonuclease treatment (QIAGEN), or using PicoPure™ RNA isolation kit (Thermofisher). RNA quality and quantity were assessed spectrophotometrically by Nanodrop 1000 (NanoDrop Technologies). cDNA was synthesized using *iScript* cDNA Synthesis kit from Bio-Rad. Real-time RT-PCR was performed using TaqMan probes, and selective primer sets described in the key resource table.

Gene expression values were calculated based on the ΔΔCt method (Livak and Schmittgen, 2001). For initial assessment of gene expression changes in mice each group consisted of 10 mice (per diet and per sex). For rats: 5 males were included in each diet group, and 11 females were included in the chow group and 12 in the HFSD group.

Drugs

Rat IL-6, or leptin, (Peprotech, Inc. United Kingdom) were dissolved in artificial cerebrospinal fluid, aCSF (Tocris, United Kingdom).

Intracranial cannulation and injections

Intra-lPBN cannulation and injections were performed in male rats. Guide cannula (26 gauge; Plastics One, USA) targeting the lPBN was implanted under ketamine: xylazine (3:1 mix; dosage 0.4 ml/240 g) anesthesia. Cannulas were secured on the skull using stainless steel screws and dental cement. The coordinates for cannula implants were 2.0/-9.2/4 mm (midline/bregma/skull, respectively) (Richard et al., 2014). The injector was aimed 6.5 mm ventral to skull. LPBN-targeted unilateral infusions of IL-6 (0.2 μg in aCSF), leptin (0.1 or 1 μg in aCSF) or aCSF were performed with a 0.5 μl injection volume at the rate 1 μl/min using a micro-infusion pump. For synergy experiments, subthreshold doses of leptin and IL-6 (0.1 μg for both drugs) were used; these doses are based on the feeding effect of both ligands. For the combination of leptin and IL-6, premixed leptin and IL-6 were delivered. All injections were performed in a counterbalanced Latin square design, where each animal received each treatment. Each injection day was separated by at least 48. Cannula placements and injectate volume spread were confirmed using 15μM brain sections, fixed and stained with DAPI and observed under epifluorescence microscope. Rats with cannulas outside of the lPBN were eliminated from the study.

lPBN IL-6 gene knockdown

AAV construct iAAV01087702 (IL-6 AAV siRNA pooled virus Serotype 2) and control construct iiAAV01502 (Scrambled AAV siRNA control virus Serotype 2) titer 10^{12} GC/ml were purchased from ABM (Richmond, Canada). Both constructs contain EGFP fluorescent markers. AAVs were injected at the rate of 0.1 μl/min (0.4 μl per hemisphere), using the lPBN coordinates as described above, and the injectors were left in place for 10 min post-injection to allow diffusion away from injection site. Food intake and body weight of the rats were followed daily for four weeks (n = 17 for each treatment group). Following the four-week period of undisturbed intake and weight measurements, body temperature (n = 8 in each group), home-cage activity (n = 8 in each group), BAT temperature (n = 8 in each group), and anxiety-like behavior were tested as described above. For terminal tissue collection, rats were decapitated under isoflurane anesthesia and brain and adipose tissues were collected and stored in $-80 °C$ freezer for immunohistochemistry or gene expression analysis.

Acute food intake measurements

Acute effect of IL-6 injections on food intake was measured in lean (n = 13) and HFSD-fed rats (n = 9). For lean rats the intake was measured at 1 and 6h, and for HFSD-fed rats intake of lard, chow, and sucrose solution (all foods were a part of the HFSD maintenance diet) was measured at 6h after injections. In both groups injections and measurements were done during light phase. The HFSD-fed rats were on the diet for 3 weeks at the time of testing. For assessment of the intra-PBN leptin injections, chow intake was recorded via automated feedometers that continuously measured food intake to the nearest ± 0.1 g/m/24h. Six rats were tested in the feedometers, and injections were applied in a counterbalanced

Telemetric measurements

For continuous, home-cage, measurements of core temperature, activity and heart rate with telemetric transponders, a small lateral incision was made and the transmitter was implanted in abdominal cavity. For heart rate measurements two subcutaneous leads were positioned on either side of the heart and sutured to the chest muscles. The body of the transmitter was sutured to the abdominal muscle to secure its position. The skin was closed using sterile non-absorbable silk suture. Rats were allowed to recover for at least five days post-surgery. For central IL-6 injection experiments (Figure 2), rats (n = 8) were implanted with an intraperitoneal telemetric radio transmitter, E-mitter-G2 (Minimitter, OR) and immediately after brain guide cannula placement surgery. For experiments with central injections of leptin (Figure 3) HRC 4000 VitalView (Minimitter, OR) were utilized (n = 18).

Brown adipose tissue (BAT) temperature measurements

Skin temperature above the BAT region was measured using FLIR T500-Series thermal camera and analyzed using FLIR tools software as previously described (Lee et al., 2018; Martinez-Sanchez et al., 2017; Matesanz et al., 2017) (n = 7 for IL-6 injections, n = 12 for the leptin/IL-6 interaction experiment). The infrared camera was utilized for measuring skin temperature directly above the BAT region of the rats. Preliminary observations indicated that more reliable results are obtained when the skin region above BAT is not covered by fur, therefore a defined region above BAT was shaved two days before obtaining thermal images. Four to five consecutive images were taken in the home-cage environment per rat from a fixed distance and the average temperature was used for data analysis. Additionally, to assess the possibility of cooperative or opposing (to the changes in core temperature driven by BAT) changes in tail blood perfusion, infrared images of the tails were taken, and tail surface temperature was scored at the mid and tip level of the tail.

Anxiety-like behavior evaluation

Standard elevated plus maze (EPM) apparatus for rats (Med-Associates, Georgia, VT, USA) (n = 7 in each group) or open field apparatus (n = 8 for controls and n = 7 for kd) for rats was utilized for quantifying anxiety like behavior. EPM was placed 70 cm above ground, consisted of two open arms, 50 × 10 cm, and two closed arms 50 × 10 × 40 cm and a central square platform 10 × 10 cm. Rats were acclimatized to the EPM room for 30 minutes and then placed on the central platform and allowed to move freely for 5 minutes. The amount of time spent on each arm was detected by measuring beam breaks of infrared lasers and recorded with MED-SYST-8A PCI operating and software package, provided by Med-Associates. The apparatus was cleaned with water between each test subject. Immediately post EPM, the rats were placed in a brightly lit arena (90 × 90 × 30 cm, Med-Associates, VT, USA) for 15 minutes for the open field test. The open field chambers were equipped with a grid of photocells for detecting movement. Photocells were coupled to a computer-based system that registers movements and time spent in each section (center or periphery) of the arena. Both EPM and open field were carried out during the light cycle.

Acute Stress

Restraint stress was used to test whether acute stress leads to increased lPBN IL-6 mRNA level and lPBN of the stressed (n = 7) and control (n = 8) rats was collected for gene expression analysis. Rats in the acute stress group were restrained for 30 minutes (tests performed in the light cycle between 09:00 and 15:00 hours) in standard restraining devices (Maniscalco et al., 2015; Ulrich-Lai et al., 2010, 2011, 2015), while control rats were left undisturbed in their home cages. Immediately following acute stress the rats were anesthetized using isoflurane followed by decapitation. The brains were then quickly removed and flash frozen using isopentane on dry ice.

Blood biochemistry

Plasma levels of TSH, T3 and T4 in control and lPBN IL-6 knockdown rats (n = 8, each) were measured using rat ELISA kits (López et al., 2010; Martinez-Sanchez et al., 2017; Varela et al., 2012). Trunk blood was collected in regular Eppendorf tubes and spun at 10 000 rpm for 10 minutes and the top layer (plasma) was transferred to a new tube and stored in −80°C. Levels of TSH, T3 and T4 were measured using rat ELISA kits (Crystal Chem, Illinois, USA. Total T3 ELISA/T4 ELISA/TSH ELISA kits are competitive ELISAs for T3/T4/TSH. We utilize a labeled antigen conjugated with an HRP and a monoclonal T3/T4/TSH antibody bound through a secondary antibody on the microplate wells. The unlabeled antigen present in the test samples and standards is incubated in microplate with HRP labeled antigen. Both labeled and unlabeled antigens compete for binding to the T3/T4/TSH antibody immobilized to the microplate. After incubation, all unbound antigens are removed via a wash step. Subsequently, a substrate solution and stop solution are added, and T3/T4/TSH levels of the samples were measured by color intensity.

Brown adipose tissue immunohistochemistry

BAT tissue tyrosine hydroxylase (TH) immunohistochemistry was performed in knockdown (n = 14) and control (n = 13) rats since the knockdowns showed a reduced BAT temperature and downregulation of thermogenesis related genes. BAT tissue was cut in 8 μm sections and placed on glass slides to dry for 30 minutes at room temperature. The tissue was then fixed using 10% buffered formalin (VWR Chemicals, Stockholm, Sweden) for 10 minutes, washed with tris buffered saline (1x, 5 minutes), quenched with 3% hydrogen peroxide in methanol (20 minutes), and washed in TBS (2x). Tissue permeabilization was done using 500 μl of TBST 0,1% (tween 20) for 20 minutes. After permeabilization, blocking was performed using 1% BSA in TBST 0.1, 5% secondary host serum (goat serum) and TBST for 1 hour. Additional blocking with Avidin (15 minutes) + Biotin (15 minutes) (Avidin/Biotin blocking kit, SP-2001, Vector

lab., Inc, CA) was performed. Post-blocking, 200 μl of 1:150 TH primary antibody (BioSite Cat#LS-B3443) was added to each slide, except for negative controls, and left overnight at 4°C. Primary antibody was washed off using TBST 0.1% (4x) and secondary antibody (1:400 dilution, biotinylated anti-rabbit, goat source, BA-1000, Vector lab., Inc, CA) was then added to each slide, including negative controls, and left for 30 minutes. After TBST wash (4x), ABC mix was added to each tissue slide and incubated for 40 minutes at room temperature. DAB substrate (DAB substrate kit, ab64238, Abcam) was used for development in PBS (pH 7.4). Dehydration was performed with ethanol (70, 95 and 100%) and xylene (1 minute each). Entellan new (Merck, Cat#107961) was used as a mounting medium. Images were analyzed using image thresholder and expressed as % area of total area using IMAGEJ (https://imagej.nih.gov/ij/).

In situ hybridization using RNAScope

In situ hybridization for IL-6 mRNA using RNAscope Multiplex Fluorescent kit (Advanced Cell Diagnostics) was utilized to detect IL-6 in brain tissue. To determine IL-6 presence in neuronal, glial, or microglial cells, IL-6 mRNA and mRNA for established markers of each cell type were assessed using RNAscope. Briefly, 10-week-old male rats were sacrificed and their brains were flash frozen. Twelve μm thick lPBN-containing brain sections were cut and fixed in 10% formalin (Thermofisher scientific, Waltham, MA) for 30 minutes on ice. Following two quick washes in PBS, brain slices were dehydrated in 50% (5 minutes), 70% (5 minutes) and 2x100% (5 minutes each) ethanol and treated with protease solution (pretreatment IV, ACDbio kit) at room temperature for an hour. The protease was washed away with PBS for a total time of 15 minutes. Target probes and negative control probes were applied directly on the sections to cover them completely and incubated at 40°C for 2 hours in the HybEZ oven. Next, slides were incubated with preamplifier and amplifier probes (AMP1, 40°C for 30 minutes; AMP2, 40°C for 15 minutes; AMP3, 40°C for 30 minutes). Next, slides were incubated with fluorescent labels (AMP4-Alt A or Alt C). Finally, brain sections were incubated for 30 s with DAPI and mounting medium for fluorescence (VECTASHIELD, USA). Fluorescent images of the lPBN were captured with 40x water immersion magnification lens using LSM700 Zeiss confocal microscope and processed using Zen lite software. Approximate quantification strategy, described previously (Timper et al., 2017), was performed on 320 × 320 μm sections of the lPBN. Sections for three male rats were processed for each cell type marker and IL-6. In short, a border of 2 μm was drawn around all nuclei in the obtained images and the cells outlined in this manner were scored for absence or presence of the *in situ* signal for *Il-6* mRNA, or the three respective neuronal markers. An average number of *IL-6* mRNA positive cells was confirmed to be similar for each of the cell type markers tested (∼30% of cells were IL-6 positive), to ensure IL-6 detection consistency when combined with different *in situ* probes.

RNAScope for fixed frozen sections

Twenty μm thick perfused brain sections were air-dried for 30 minutes. Target retrieval was performed where brain sections were incubated at 99°C in a Retrieval Solution for 7.5 minutes (ACDbio), washed 3-5 times with milliQ water and dehydrated for 15 s in 100% ethanol. Protease 3 (ACDbio) was applied for 1 hour at 40°C in the HyBEZ oven. The protease was washed off with milliQ 3-5 times. Target probe for IL-6 (Rn-IL-6-C3 427141-C3) and negative control probes were applied directly on the sections to cover them completely and incubated at 40°C for 2 hours in the HybEZ oven. Next we applied preamplifier and amplifier probes (AMP1, 40°C for 30 minutes; AMP2, 40°C for 15 minutes; AMP3, 40°C for 30 minutes; AMP4-Alt B for 15 minutes). Finally, brain sections were incubated for 30 s with DAPI and mounting medium for fluorescence (VECTASHIELD, USA). Fluorescent images of the lPBN were captured under with 40x water immersion magnification lens using LSM700 Zeiss confocal microscope and processed using Zen lite software.

Acute cold exposure

Chow (n = 9 and n = 6 for control and cold-exposed respectively) or HFD-fed (8-week period; n = 10 and n = 6 for control and cold-exposed respectively) male mice were housed at 4 °C for 48h in cold chamber (Memmert HPP 750). To determine whether the effect of cold is robust and translates across species in a second experiment male (n = 6 per each temperature condition) and female (n = 7 per each condition) rats were also tested with ambient cold exposure. Sacrifice and brain collection were performed as described above.

Cold exposure in mice

Male mice fed either HFD or chow for 8 weeks were acutely exposed to 4 °C for 48 hours in their respective home cages.

Cold exposure in rats

A stepdown cold exposure protocol was utilized for rats. In brief, the temperature was decreased gradually from room temperature to 4°C in 6 hours, following which the temperature remained at 4°C for the rest of the period (48 hours in total). Control rats were housed at room temperature.

Immediately after cold exposure rodents were anesthetized using isoflurane followed by decapitation. The brains were quickly frozen using isopentane on dry ice and stored at −80 °C. Tissue punches of PBN were collected in a Leica 3050S cryostat.

Protein extraction and western blot

Interscapular BAT was dissected immediately after sacrifice, frozen in liquid nitrogen and then stored in -−80°C. Protein extraction was performed using Cell lysis buffer (Cell Signaling) with added protease inhibitor. Next, tissue was mechanically lysed using steel

beads at 2Hz for 2 minutes; the mix was left on a shaker for 2 hours at 4°C and spun at 12000 rpm for 20 minutes. Protein concentrations were determined with Bradford assay. Laemmli loading buffer and beta-mercaptoethanol mix was added to the samples, the mix was heated at 95°C for 5 minutes, and fractionated by gel electrophoresis on 4%–20% (vol/vol) Stain free gel (Biorad). Proteins were transferred on polyvinyldifluoride membranes using the Trans-Blot Turbo Transfer Pack (Biorad). Blocking of membrane was performed with filtered 5% BSA (wt/vol) in TBS–Tween 20 buffer (TBST, 10 mM Tris, 150 mM NaCl, and 0.1% Tween 20, pH 8.0) for 1 hour. Following two TBST washes, the blots were incubated with primary antibody Ucp-1 ab10983 (Abcam; 1:1000 dilution) overnight at 4°C. The membranes were washed four times for 15 minutes in TBST and incubated with secondary antibody (Anti-rabbit IgG HRP-linked antibody; catalog #7074 Cell Signaling) for 1 hour. Protein bands were developed using Pierce ECL Western Blotting Substrate and visualized with Chemidoc System from Biorad. Band analysis was performed using Image Lab program provided by Biorad.

Neural tract tracing: Brain tissue preparation and imaging

For retrograde adeno-associated virus vector (AAV)-assisted neural tract tracing, retrograde AAV vector expressing EGFP under the enhanced synapsin promoter; AAV2(Retro)-eSyn-EGFP was injected unilaterally to the PVH of two rats. Three weeks after viral infusions, rats were perfused, brains were isolated, sectioned and processed for *IL-6* (using *in situ* hybridization protocol) and DAPI. EGFP (green), RNAscope IL-6 signal (red), and DAPI (blue) were visualized and captured with a confocal microscope.

In detail: Volume of 0.5 μL of AAV2(Retro)-eSyn-EGFP (1.2x10^13 GC/ml) (Vector Biolabs, Malvern, PA, USA) was unilaterally injected at a speed of 0.1μl/min into the PVH using a Hamilton Neuro 10 μL syringe with a 33 gauge needle, the needle was left in place for 10 min to allow diffusion of the viral vector (Hamilton Co. Reno, NV, USA) PVN was targeted using the following coordinates in relation to the bregma and skull surface: anterior-posterior: −1.6 mm and mediolateral: −0.3 mm and −8.3 mm dorsal. Three weeks after viral infusions, animals received a terminal dose of a mixture of ketamine:xylazine prior to perfusion. For perfusion, the heart was exposed and prepared with a cannula attached to a perfusion pump (Watson 120S, Watson-Marlow Fluid Technology Group, Wilmington, MA, USA). Cold saline solution was circulated for 3-4 minutes at a rate of 60 ml/min and then ice –cold filtered 4% paraformaldehyde-PBS solution was ran at a volume equal to the body weight. Brains were isolated and incubated in 15% Sucrose 4% PFA-PBS solution overnight and placed in 30% sucrose-PBS solution until saturation. Samples were frozen on CO_2-ice prior to brain sectioning with a Leica 3050S cryostat (Leica Biosystems Nussloch GmbH, Nussloch, Germany). 20 μm coronal slices were collected on SuperFrost+ sample glasses (Thermo scientific, Waltham, MA, USA) and stored at - 80°C. For co-localization of *IL-6* mRNA and the retrograde EGFP signal, 20 μm thick sections were processed as described above in RNAScope for fixed frozen sections. Images were captured using a Zeiss LSM700 confocal microscope (Carl Zeiss Microscopy GmbH, Jena, Germany). Tiles images of 10x (air) and 40x (water immersion) were taken throughout the PBN in multiple layers with a depth of 1-3 μm (5-6 levels) in order to convert the images with the Maximum Projection-software (Zen software, Carl Zeiss Microscopy GmbH, Jena, Germany) for increased depth range. Coronal brain atlas figures (Paxinos & Watson 6th edition) were superimposed on the fluorescent images of the PBN sections (sections throughout the PBN were analyzed from two male rats).

QUANTIFICATION AND STATISTICAL ANALYSIS

All the data are presented as mean ± SEM. Statistical significance was analyzed using Student's t test for comparisons of two groups, or one- or two-way ANOVA with post hoc Sidak's tests when appropriate (GraphPad Software, Inc). $p < 0.05$ was considered statistically significant.

Supplemental Information

Parabrachial Interleukin-6 Reduces Body Weight

and Food Intake and Increases Thermogenesis

to Regulate Energy Metabolism

Devesh Mishra, Jennifer E. Richard, Ivana Maric, Begona Porteiro, Martin Häring, Sander Kooijman, Saliha Musovic, Kim Eerola, Lorena López-Ferreras, Eduard Peris, Katarzyna Grycel, Olesya T. Shevchouk, Peter Micallef, Charlotta S. Olofsson, Ingrid Wernstedt Asterholm, Harvey J. Grill, Ruben Nogueiras, and Karolina P. Skibicka
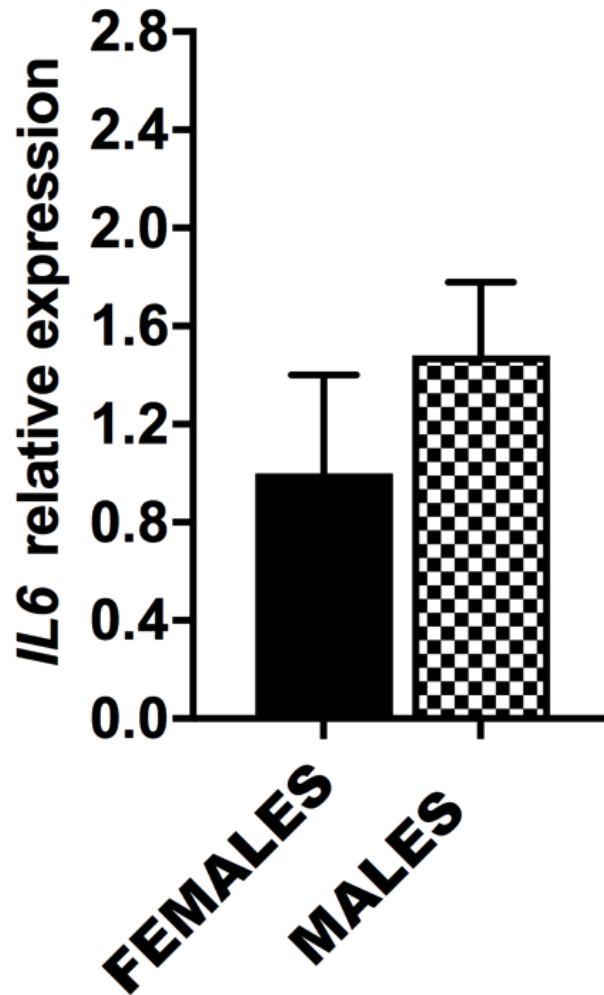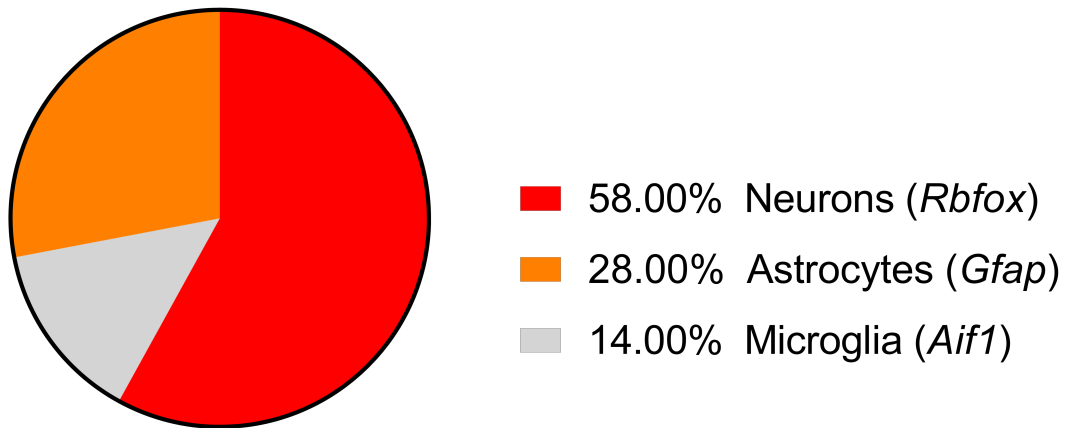
SI

Figure S1: Comparison of IL-6 gene expression levels in chow-fed 13-week-old male and female mice (see figure 1 in the main text) in the parabrachial nucleus. Expression levels were detected by quantitative real-time PCR. Unpaired Student's t-test n=10 males and n=6 females.
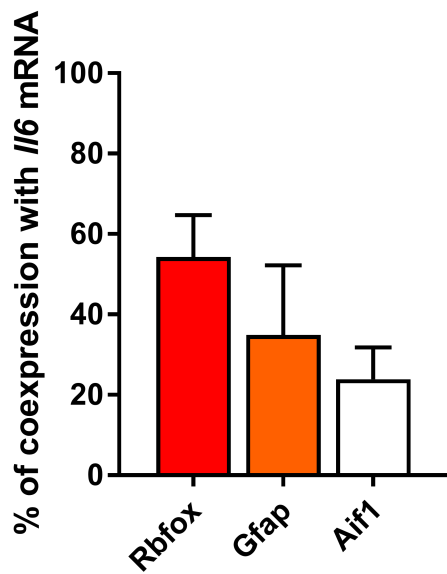
A

■ 58.00% Neurons (*Rbfox*)

■ 28.00% Astrocytes (*Gfap*)

□ 14.00% Microglia (*Aif1*)

B

Figure S2: **Results of approximate quantification of co-expression of cellular markers with IL-6 mRNA in the lPBN of chow-fed 10-week-old male rats. Related to Fig 1Q-S in the main text.** (A) Diagram illustrating the proportion (by %) of IL-6 mRNA expressed by neurons, astrocytes, and microglia. (B) Proportion (by %) of each cell type co-expressing IL-6 mRNA at bregma -9.2 mm level. For Rbfox and Gfap experiments, the lPBN from three male rats was used, Aif1 counts are taken from two rats since the third rat lPBN showed levels of Aif1 close to that of negative control. Data represent mean ± SEM.
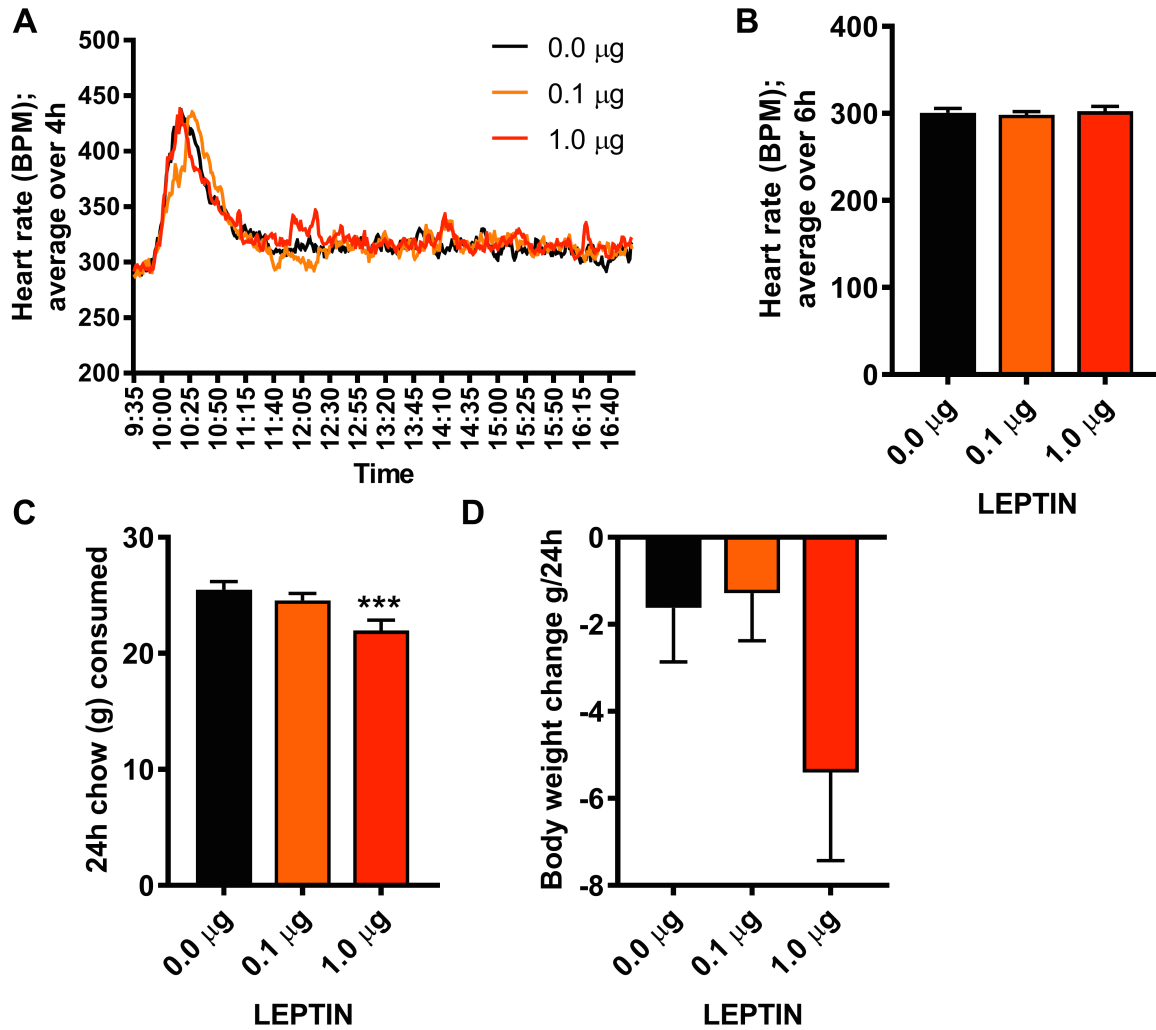
Figure S3: **Measurement of lPBN leptin-administration on cardiovascular activation, feeding and body weight. Related to Fig 3 in the main text.** Heart rate, food intake and body weight gain were monitored after intra-lPBN leptin injections in chow-fed male rats. (A) Line graph derived from continues telemetric hear rate monitoring in male rats. 10.00 injection time. (B) Heart rate averaged over 6h post-injection period. (C) Chow intake 24h after leptin injection (18h after food was offered since food was not available during telemetric recordings). (D) Body weight change in male rats after leptin administration during the light phase. Data represent mean ± SEM. ***$P<0.001$. One-way ANOVAs were used followed by Sidak's post-hoc test.
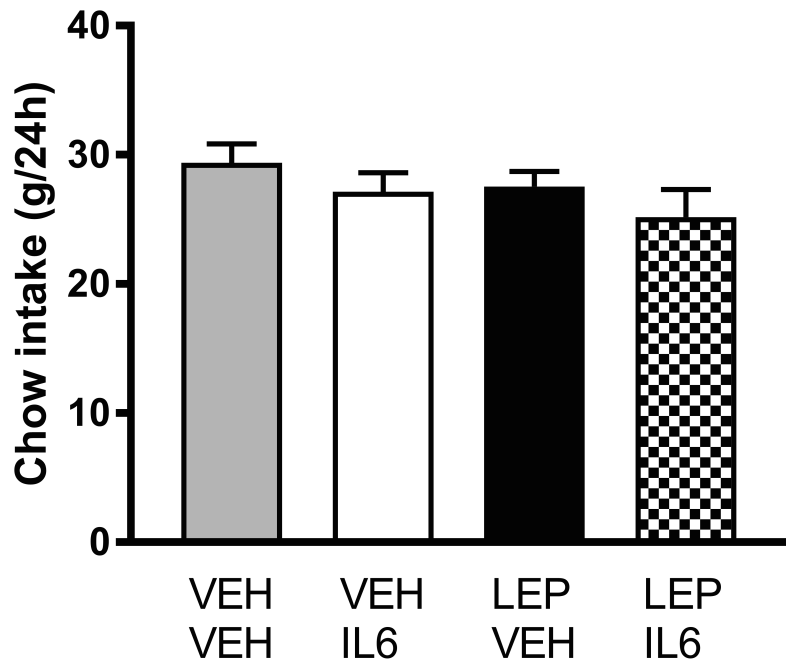
Figure S4. Effect of subthreshold doses of leptin and IL-6 on 24h food intake in male rats. Related to Fig 3. Subthreshold doses of IL-6 and leptin alone, or in combination, were injected into the lPBN of male chow-fed rats and cumulative 24h chow intake was measured (two-way ANOVA, n=12). These rats were 11 weeks old during experimentation.
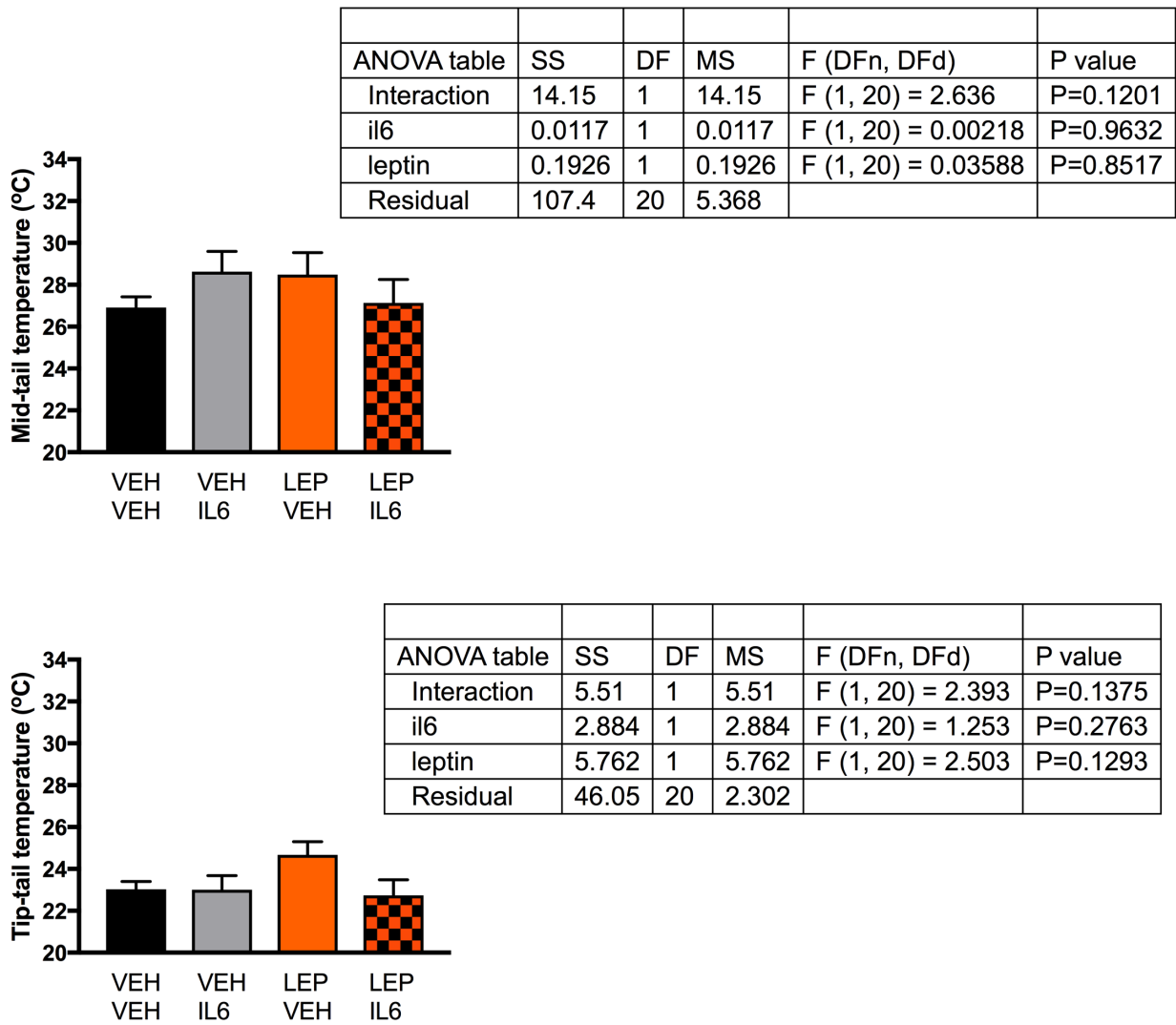
ANOVA table	SS	DF	MS	F (DFn, DFd)	P value
Interaction	14.15	1	14.15	F (1, 20) = 2.636	P=0.1201
il6	0.0117	1	0.0117	F (1, 20) = 0.00218	P=0.9632
leptin	0.1926	1	0.1926	F (1, 20) = 0.03588	P=0.8517
Residual	107.4	20	5.368		

ANOVA table	SS	DF	MS	F (DFn, DFd)	P value
Interaction	5.51	1	5.51	F (1, 20) = 2.393	P=0.1375
il6	2.884	1	2.884	F (1, 20) = 1.253	P=0.2763
leptin	5.762	1	5.762	F (1, 20) = 2.503	P=0.1293
Residual	46.05	20	2.302		

Figure S5: Effect of leptin and IL-6 on tail surface temperature in male rats. Related to Fig 3, new cohort of rats was used for this study. IL-6, or leptin each applied at a dose of 0.1 µg, or the combination of the two substances was delivered into the lPBN of male chow-fed rats. Tail temperature was measured here at mid and tip sections of the rat tail with the FLIR infrared imaging. Data represent mean ± SEM, for detailed statistics see tables embedded in this figure.
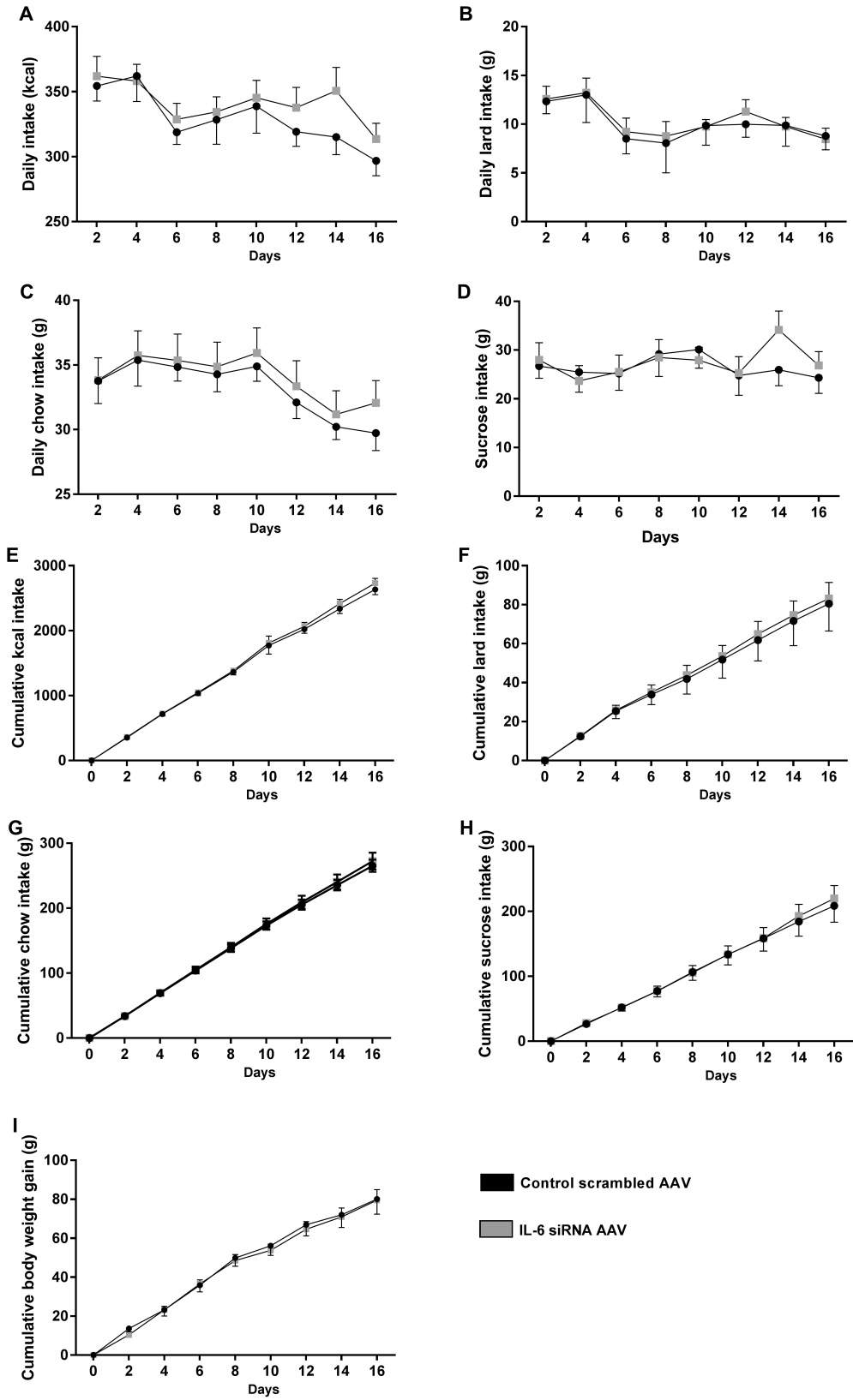
A — Daily intake (kcal) vs Days

B — Daily lard intake (g) vs Days

C — Daily chow intake (g) vs Days

D — Sucrose intake (g) vs Days

E — Cumulative kcal intake vs Days

F — Cumulative lard intake (g) vs Days

G — Cumulative chow intake (g) vs Days

H — Cumulative sucrose intake (g) vs Days

I — Cumulative body weight gain (g) vs Days

Control scrambled AAV

IL-6 siRNA AAV

Figure S6: I**nactive (light) period intake was selectively affected by the lPBN kd in rats fed an obesogenic diet (see Figure 4 I-M), however the overall 24h intake, shown here, was not affected**. AAV-delivered siRNA was utilized to achieve IL-6 knockdown in the lPBN of male rats (as shown in figure 4) offered high-fat/high-sugar choice diet. (A) Daily caloric intake, (B) lard intake, (C) chow intake, (D) and sucrose intake were measured for the first 16 days on the diet. (E-H) Cumulative analysis of intake. (I) Cumulative weight gain. Note that for the high-fat/high-sugar diet feeding experiments, the rats were placed on the diet at least four weeks after AAV-siRNA infusions, thus there was sufficient time for the AAV siRNA to knockdown the gene of interest. Two-weeks of diet exposure are shown here; the rats were followed for a total of four weeks without any changes between the scrambled and IL-6 kd detected. Two-way ANOVA for cumulative comparisons with Sidak's post-hoc test. n=10-12.
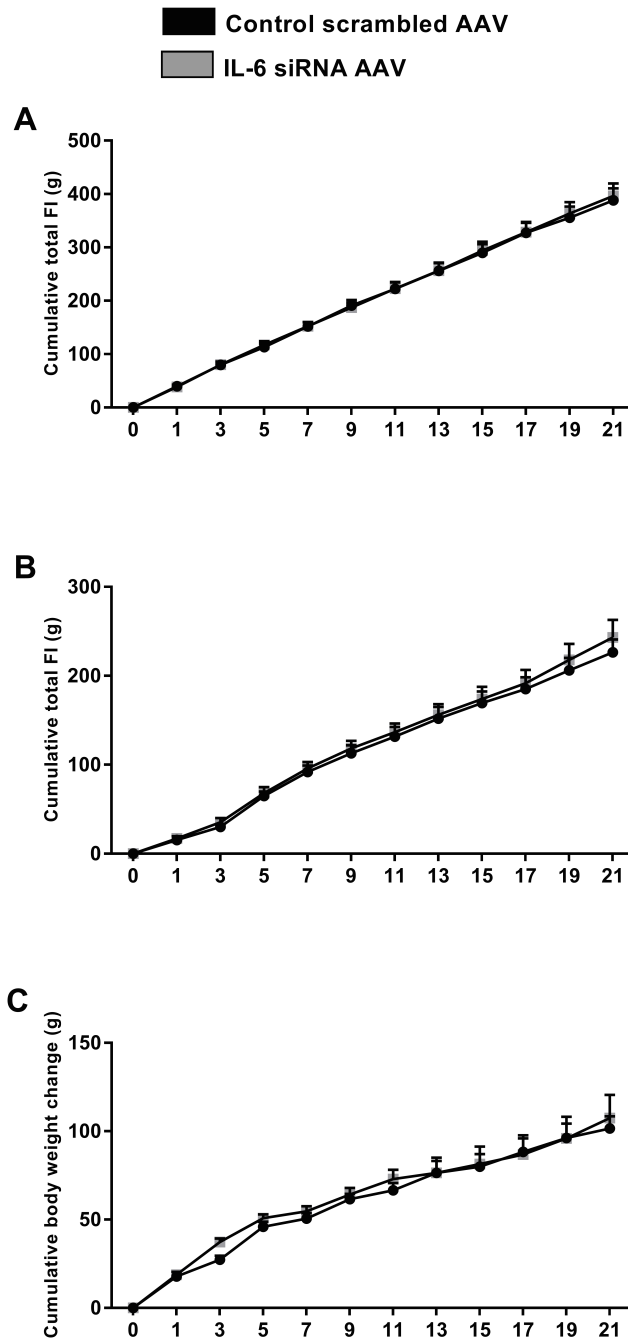
Figure S7: **Unlike the chow-fed IL-6 kd rats, rats fed the high-fat/high-sugar diet, did not gain more weight or did not display chronic daily hyperphagia when maintained on the palatable diet.** Related to fig 4 in the main text. The first diet offered a free choice of lard as solid, and sugar, as a sucrose solution, and chow (see Fig S6). In order to determine whether the lack of weight gain was driven by the specific diet used, a new group of rats, with lPBN IL-6 kd, was offered a different diet, where sugar and lard were mixed (1:1 by weight) and provided in a solid form in addition to water and chow. (A) Intake of chow or (B) the palatable mix, and (C) body weight were measured for 3 weeks. 2-way ANOVA, Sidak's post-hoc test with n=9 in each group. FI, food intake.

Mishra et al 2019, *Cell Reports*